Design and Analysis of a Bidirectional Rack and Pinion Wave Energy Converter (WEC)

A thesis proposal presented to the faculty of the Graduate School of Western Carolina University in partial fulfillment of the requirements for the degree of Master of Science in Technology

By
Md Shohel Amin

Director: Dr. Bora Karayaka
Associate Professor
School of Engineering and Technology

Committee Members:
Dr. Paul Yanik, School of Engineering and Technology
Dr. Yuanrui Sang, Department of Electrical and computer Engineering

June 2021

©2021 by Md Shohel Amin

ACKNOWLEDGEMENTS

I am very proud of being a part of Western Carolina University. The faculty members immensely supported me towards attaining my degree. They also enriched my knowledge and enhanced my enthusiasm to acquire more knowledge.

I specially want to thank Dr. Bora Karayaka for his extensive support to my research. He opened the arena of ocean wave energy converter research towards me. I considered myself very lucky to work with him in this research sector. His dedication of research inspires me to give my best effort to my work. He is always friendly and helpful. I am blessed to have him as my thesis supervisor.

I also want to thank my committee member Dr. Paul Yanik and Dr. Yuanrui Sang for their collaboration of my research. I also want to thank my graduate classmate for their help and friendly attitude.

Finally, I want to thank to my family for their patient, love, and support.

TABLE OF CONTENTS

LIST OF TABLES iv
LIST OF FIGURES v
ABSTRACT vi
CHAPTER 1: INTRODUCTION 1
CHAPTER 2: LITERATURE REVIEW 4
2.1 Overall System Model 4
2.2 Hydrodynamic Model 6
2.3 Power Take Off System Model 10
CHAPTER 3: METHODOLOGY 11
3.1 Electrical Analogue of the Equivalent Mechanical System 11
3.2 Operating Principles of the Rack and Pinion based WEC 13
3.3 Control Mechanism of The Rack and Pinion WEC 14
3.4 Unidirectional Rotation of Pinion and Generator Shaft 15
3.5 Synchronism between wave excitation force and generator shaft speed 15
3.6 Irregular wave processing methodology 15
CHAPTER 4: RESULTS AND DISCUSSION 19
4.1 Theoretical Calculation of Maximum Energy Extraction 19
4.2 WEC Model with a DC machine under regular wave conditions 21
4.2.1 Simulation Model 21
4.2.2 A Simulation Example 23
4.2.3 The Effect of Scaling Factor and Gear Ratio 25
4.2.4 The Effect of Gear Ratio and Generator Moment of Inertia 26
4.2.5 The Effect of Passive load (Resistor) 27
4.3 WEC Model with a DC machine under irregular wave conditions 28
CHAPTER 5: CONCLUSION AND FUTURE WORK 36
REFERENCES 38
Appendix 41
APPENDIX A: SOURCE CODE 42
APPENDIX B: WEIGHTED POWER RESULTS WITH IRREGULAR WAVES 58

LIST OF TABLES

Table 3.1:	Equivalent mechanical quantities to electrical quantities.	12
Table 3.2:	Six sea states that are selected for real wave environment.	18
Table 4.1:	Theoretical energy extraction in rms value.	20
Table 4.2:	Mechanical/Hydrodynamic parameters used in simulation.	22
Table 4.3:	Permanent magnet DC machine parameters used in simulation.	23
Table 4.4:	Average electrical power at different scaling factor and gear ratio for wave period 5s, 8s, and 10s.	25
Table 4.5:	Maximum average electrical power at different gear ratio and inertia.	26
Table 4.6:	Average electrical energy extraction using passive load.	29
Table 4.7:	Energy extraction at different gear ratio and scaling factor for irregular wave.	29
Table 4.8:	Peak current for inertia 0.5 $kg.m^2$ at gear ratio 1.5 and 1/5000 scaling factor	35
Table 4.9:	Peak current for inertia 0.5 $kg.m^2$ at gear ratio 2.5 and 0.45/5000 scaling factor	35
Table B.1:	Weighted power extraction of six sea states for inertia, J=1.5 $Kg.m^2$	58
Table B.2:	Weighted power extraction of six sea states for inertia, J=1.0 $Kg.m^2$	59
Table B.3:	Weighted power extraction of six sea states for inertia, J=0.5 $Kg.m^2$	60

LIST OF FIGURES

Figure 2.1:	The overall system of rack and pinion mechanism.………………….	04
Figure 2.2:	An example of JONSWAP spectrum……………..………………….	08
Figure 3.1:	Equivalent electrical analogue of the hydrodynamic system.….…….	11
Figure 3.2:	Block diagram of the control system.……………………….….….	14
Figure 4.1:	(a) Wave Excitation force (b) buoy velocity (c) generator shaft speed (blue) and pinion speed (red)..……………………….…….….	17
Figure 4.2:	Weighted Electrical power extraction for inertia, J=1.5 $kg.m^2$………	31
Figure 4.3:	Weighted Electrical power extraction for inertia, J=0.5 $kg.m^2$………	32
Figure 4.4:	Percentage efficiency of power for IWS 4 at inertia, J=0.5 $kg.m^2$…...	33
Figure 4.5:	Percentage efficiency of power for IWS 4 at inertia, J=0.5 $kg.m^2$...…	34
Figure A.1:	Simulink Model for regular waves…….…………………….….….	45
Figure A.2:	Details of F_pto block for regular waves…………………….……..	46
Figure A.3:	Simulink Model for irregular waves….…………….……….….….	56
Figure A.4:	Details of F_pto block for irregular waves...………….………..…….	57

ABSTRACT

DESIGN AND ANALYSIS OF A BIDIRECTIONAL RACK AND PINION WAVE ENERGY CONVERTER (WEC)

Md Shohel Amin, M.S.T

Western Carolina University (April 2021)

Director: Dr. Bora Karayaka

Ocean wave energy is becoming very popular among all the current renewable energy sources because of its cleanliness, availability, high power density and pollution free nature. Many wave energy converters have been designed and analyzed with various power take off systems like air turbines, hydroelectric components, and slider crank. In this thesis, the easiest and most effective method of using rack and pinion type power take off system, is discussed and the performance of the whole system is analyzed. The bidirectional motion of the pinion is converted into unidirectional motion by applying ratcheting method. This increases the overall efficiency of the system. A wave energy converter containing buoy and a mechanical motion rectifier (MMR) based rack and pinion are proposed to be designed and simulated in MATLAB Simulink environment. This system mainly consists of a buoy that is semi-submerged into the water. The ocean waves exert force on the submerged buoy. The up and down movement of the buoy is then converted into unidirectional rotation by rack and pinion mechanism. Through a gear box this rotational motion drives the generator to produce electricity. The control strategy keeps the generator's velocity and wave excitation force in resonance. Here, a time domain system analysis method is applied for solving the equation that describes the relationship between the buoy motion and hydrodynamic forces in both cases of regular wave and irregular waves. The simulation results for the regular and irregular ocean waves are presented and compared with other state-of-the-art power take off systems.

CHAPTER 1: INTRODUCTION

Renewable energy sources produce electricity that is both environmentally friendly and economical. Carbon dioxide is one of the leading causes of global climate change which is produced by using fossil fuel-based generation methods. Renewable energy can be one of the best solutions to produce energy without any production of carbon dioxide. Ocean wave energy is a renewable, environmentally friendly, and sustainable source of energy. The water in the ocean is always in motion which is an opportunity for engineers to convert this movement of water into electrical energy. One of the major advantages of ocean wave energy is that the production of this energy is generally more consistent and predictable than the solar and wind energy production which depend largely on the intensity of sunlight and flow of wind, respectively [1]. There is enormous energy potential in the ocean that is available all the time. The energy conversion efficiency of ocean wave energy is also higher than wind and solar [2]. It is estimated that if the ocean wave energy is fully exploited, it could satisfy 40% of the worldwide demand for power which is equal to the output power of 700 to 800 nuclear power stations. The method of extracting electrical energy from ocean waves can be classified in a few different ways. There are two main categories of ocean wave energy converter (WEC), i.e, turbine type and buoy type, which are mentioned by Muetze et al. [3]. There are also other unique types of WECs such as the Pelamis and piezoelectric materials-based converters.

Oscillating water column (OWC) is the well-developed turbine type ocean wave energy converter with simple construction. The working principle of this type of energy converter is similar to the wind energy turbine. A closed hollow air chamber is placed on seawater in such a way that the chamber is submerged into the ocean. The movement of water creates air pressure inside the chamber. A turbine is installed below the roof of the air chamber. The operation and the modeling of this kind of turbine are analyzed by Dorrell et al.'s research [4]. When the water level inside the chamber rises, it increases the air pressure. This pressured air flows through the turbine and the turbine rotates. When the water level decreases the air is then drawn back to the chamber and as a result the turbine again rotates. The turbine is designed in a way that it will rotate in only one direction regardless of the direction of the airflow.

The buoy type wave energy converter is also known as point absorber (PA). They are installed in the offshore area. Here, a buoy is placed on the top of the water level in the ocean. The buoy moves up and down according to the ocean waves. This up and down movement is then converted into rotational motion using different methods. This rotational motion is then fed to the generator turbine.

According to power take-off (PTO) systems, Liang *et al.* [5] categorized WECs into three types, i.e., air turbine, hydroelectric motor, and linear electrical generator. OWC uses the air turbine type PTO system. The air turbine has a simple construction and the power generation by this kind of turbine is easy and reliable. Pelamis WEC is an example of hydroelectric motor-based PTO. Pelamis consists of many cylindrical blocks like a linked chain. The hydraulic PTO generally exploits the high-pressured piston pumps or rotational generators for harnessing energy [6]. In a linear electrical generator, a bulk magnet is moved back and forth through a voice coil. As a result, this PTO system does not have any frictional loss.

The proposed control algorithm operates on a rack and pinion based WEC which is an oscillating body direct drive rotational (DDR) converter. In wave energy application, the DDR converter means that the buoy motion and the wave excitation force are directly applied to the generator. The energy conversion efficiency for DDR converters is proved to be higher than the linear generator system [7]. The rack and pinion based WEC coupled with a mechanical motion rectifier (MMR) can extract more power than linear PTO systems under the regular wave condition [5]. However, there was no specific control algorithm proposed in [5] to maximize the energy captured by this WEC. This paper implements a model of a rack and pinion WEC power take-off (PTO) system. Then, a suboptimal control algorithm is designed so that the system can extract the maximum possible energy. The simulated model is executed with different system parameters to analyze their effect on energy extraction and system stability.

This thesis implements a model of a rack and pinion WEC power take-off (PTO) system. Then, a suboptimal control algorithm is designed so that the system can extract the maximum possible energy. The simulated model is executed with different system parameters to analyze their effect on energy extraction and system stability.

CHAPTER 2: LITERATURE REVIEW

2.1 Overall System Model

The system model mainly consists of two racks, two pinions, a connecting rod, and a buoy that is semi-submerged into the water. The cross-sectional view of a single rack and pinion mechanism are represented by figure 2.1. The two racks are affixed to the buoy through a connecting rod and two pinions which are attached to the generator shaft. The ocean waves exert force on the submerged buoy, resulting in the two racks connected to the buoy moving up and down. The exerted force on the buoy creates sufficient torque to drive the pinions that are geared with the two racks.

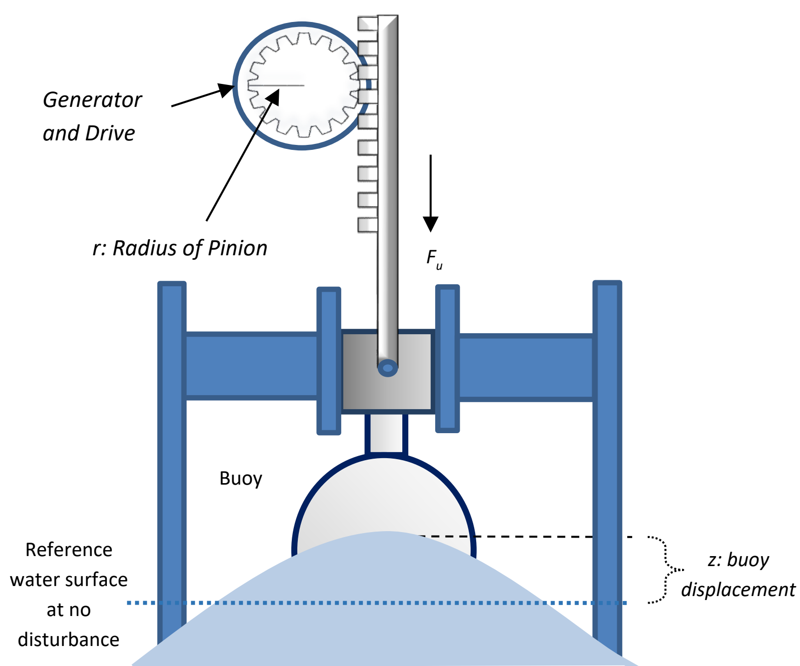

Figure 2.1: The overall system of rack and pinion mechanism

One rack and pinion pair convert the translational motion to rotate in one direction when the buoy moves up and the other rack and pinion pair converts the motion in the opposite direction when the buoy moves down [5]. The MMR rectifies this two-way rotation into a one-way rotation. Through a gearbox, the unidirectional motion then drives the shaft of a generator to produce electricity. Therefore, the PTO force will experience the engagement and disengagement of the one-way bearings. When the generator shaft speed is higher than the pinion speed, the generator becomes disengaged with the pinion. As a result, the generator shaft rotates by itself and the hydrodynamic forces applied on the generator shaft become zero as shown in (1). The load on the generator is actively controlled by applying variable voltages across the electrical machine's armature circuit. The system engages when the generator shaft speed is equal to or less than the speed of the pinion. The hydrodynamic forces are applied to the generator during the engagement. The reactionary PTO force (F_u) is described by (3). So, this force during the engagement and disengagement can be given by (1).

$$F_u = \begin{cases} 0 & \omega_s > \omega_p : \text{ disengagement} \\ F_{pto} & \omega_s \leq \omega_p : \text{engagement} \end{cases} \tag{1}$$

where, ω_s is the generator shaft speed, ω_p is the pinion speed (directly proportional to buoy velocity) and F_{pto} is the force exerted by the electrical machine given by (2).

$$F_{pto} = \frac{n_g}{r}(J\frac{d\omega_s}{dt} + B\omega_s + T_{em}) \tag{2}$$

where J is the system inertia constant in *kg/m*^{2}, B is the viscous damping constant in *Nm.s/rad*, T_{em} is the electromechanical torque developed by the machine in *Nm*, n_g is the gear ratio and r is the radius of pinion as shown in Figure 2.1.

2.2 Hydrodynamic Model

A spherical buoy is considered for the analysis, based on linear heave motion [8]. Regular waves with infinite water depth consideration are investigated and analyzed in this research. Irregular waves with significant wave height of 2m are also analyzed. Time domain analysis (Cummins equation) model is adopted to calculate the hydrodynamic force. The wave excitation force calculation for both regular wave condition and irregular wave condition will be illustrated in this section.

The Cummins equation [9] delineates the relationship between the buoy displacement and hydrodynamic forces which can be written as

$$(M + a_\infty)\ddot{z}(t) + \int_{-\infty}^{t} H_{rad}(t-\tau)\,\dot{z}(\tau)d\tau + S_b z(t) = F_e(t) - F_u(t) \tag{3}$$

In (3), z is the distance between the buoy center of gravity and the reference water level with no disturbance, M is the physical mass of the buoy, a_∞ is the buoy added mass for a semi-submerged and spherical shaped buoy at infinite wave period that is shown half of the physical mass in [10], H_{rad} is the radiation impulse response function of the buoy, S_b is the hydrostatic stiffness, F_e is the wave excitation force, F_u is the reactionary PTO force.

Equation (4) express the radiation force,

$$F_{rad} = \int_{-\infty}^{t} H_{rad}(t-\tau)\,\dot{z}(\tau)d\tau \tag{4}$$

where F_{rad} is the radiation force and $\dot{z}$ is buoy velocity. The analytical solution for the radiation force of the buoy can be found in [10].

The hydrostatic stiffness of a semi-submerged buoy with radius a can be expressed by equation (5).

$$S_b = \rho g \pi a^2 \tag{5}$$

where ρ is the density of water, g is the acceleration due to gravity and a is the radius of the buoy.

2.2.1 Wave Excitation Force Calculation for Regular Ocean Wave

The regular ocean wave is a sinusoidal wave, and its wave elevation can be shown as

$$z_w = A \cdot \sin(\omega t + \varphi) \tag{6}$$

where A is the wave amplitude, ω is the angular velocity of the wave and φ is the initial phase of the wave.

The wave excitation force in the heave direction for a semi-submerged buoy can be calculated as

$$F_e = \kappa \rho g \pi a^2 z_w \tag{7}$$

where, z_w is the elevation of the water surface and κ is the excitation force coefficient. The amplitude of κ can be determined by (8).

$$|\kappa| = \sqrt{\frac{4\varepsilon_r}{3\pi ka}} \tag{8}$$

Here, ε_r is the radiation resistance coefficient that is evaluated in [10,11]. The value of ka is considered small in this research, so the phase angle can be assumed to be zero [12].

The wave number k for infinite water depth is given in (9).

$$k = \frac{\omega^2}{g} = \frac{2\pi}{\lambda} \tag{9}$$

where ω is wave angular velocity and λ is the wavelength.

2.2.2 Wave Excitation Force Calculation for Irregular Ocean Wave

An irregular wave is the superposition of many regular waves with different wave amplitudes, angular velocities, and phase. The angular velocity is utilized between 0.1 radian/s to

2 radian/s which is denoted by Δf with an interval of 0.01 radian/s in this research. The amplitudes of the irregular waves were generated by JONSWAP spectrum.

The equal energy transport theorem [13] assists selecting the significant wave height to compare energy extraction between regular waves and irregular waves.

$$H_{m0} = 2\sqrt{2}A \tag{10}$$

Where A is the amplitude of the regular ocean wave with equal energy.

The JONSWAP spectrum with a significant wave height of 2 meter, a peak wave period of 10 seconds, and γ of 6 is shown in figure 2.2.

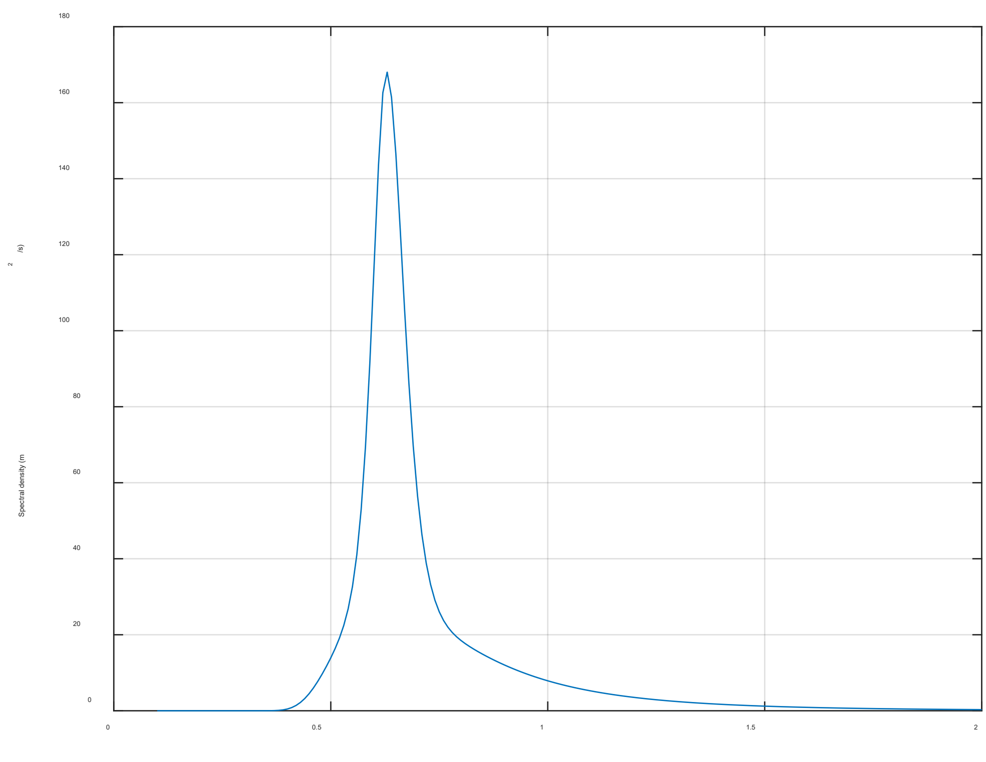

Figure 2.2: An example of JONSWAP spectrum.

The amplitude of each component of the irregular wave can thus be expressed as in [14]

$$A_i = \sqrt{2S(f_i)\Delta f} \tag{11}$$

where f_i represents each regular wave component and Δf is the difference between two frequency components.

The phase of each component of the irregular wave is randomly generated from 0 to π, and it is denoted as φ_i . Thus, the irregular wave elevation can be expressed as the summation of all the wave components

$$z_w = \sum_{i=1}^{N} A_i \cdot \sin(\omega_i t + \varphi_i) \tag{12}$$

where N is the total number of wave components, ω_i is the frequency of wave component in radian/second and φ_i is the phase angle for each wave component in radian.

So, the wave excitation force due to irregular wave is calculated as

$$F_e = |\kappa| \rho g \pi a^2 z_w \angle \varphi_\kappa \tag{13}$$

where z_w is the water surface elevation, κ is the excitation force coefficient [15], g is the acceleration due to gravity, ρ is the density of water, and a is the radius of the buoy.

The amplitude, imaginary and real parts of κ can be determined as

$$|\kappa| = \sqrt{\frac{4\varepsilon_r}{3\pi k a}} \tag{14}$$

$$Im(\kappa) = \frac{2\varepsilon_r k a}{3} \tag{15}$$

$$Re(\kappa) = \sqrt{|\kappa|^2 - [Im(\kappa)]^2} \tag{16}$$

where, assuming infinite water depth, wave number k can be calculated as

$$k = \frac{\omega^2}{g} = \frac{2\pi}{\lambda} \tag{17}$$

The phase angle of κ can be calculated as

$$\angle\varphi_{\kappa} = atan\left(\frac{Im(\kappa)}{Re(\kappa)}\right) \tag{18}$$

2.3 Power Take Off System Model

In this research, A DC machine coupled with a resistance (passive load) and a four-quadrant DC chopper (active load) are modeled in the simulation. Resistance values ranging from 2 Ω to 20 Ω are utilized during the simulation. The DC machine is easy to model, control, and comparatively efficient with a DDR-WEC system [6]. Equation (7) and equation (13) are utilized to evaluate the wave excitation force for regular wave and irregular wave respectively. The reactionary PTO force (F_u) can be calculated using (3). If the radii of the pinions are r, then the torque that is applied to drive the generator can be calculated from (10) during engagement. Otherwise, this torque is zero.

$$T_u = F_u \cdot r \tag{19}$$

It is possible to calculate the buoy displacement (z) from the physical structure of the system model.

$$z = r \cdot \theta \tag{20}$$

where z is the buoy displacement, r is the radius of the pinion and θ is the angular displacement of the pinion.

The frequency of ocean wave generally lies between 1/5 Hz to 1/18 Hz which is 5 rpm to 18 rpm if they move rotationally. Whereas the speed of generator used in this study can reach up to more than 1000 rpm. The generator can produce little power if it is rotating at 5 rpm to 18rpm. Therefore, a gearbox is used in between the pinion and the generator shaft so that the generator can rotate efficiently to produce a substantial amount of electrical energy [16].

CHAPTER 3: METHODOLOGY

3.1 Electrical Analogue of the Equivalent Mechanical System

The linear potential flow theory describes the relationship between the excitation force, hydrodynamic force, and PTO force assuming deep water and small wave amplitude [17]. An electrical analogue for a wave energy conversion system can be introduced to model this system based on this assumption [18]. Figure 3.1 and Table 3.1 represents the correspondence between the mechanical and electrical quantities of this system [18, 13].

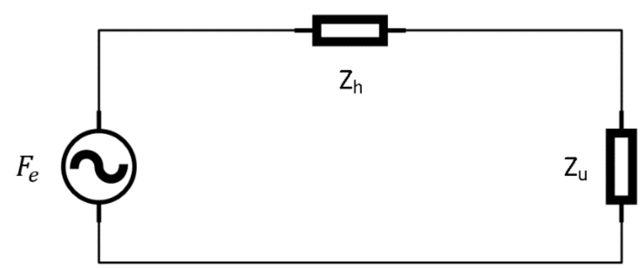

Figure 3.1: Equivalent electrical analogue of the hydrodynamic system.

The hydrodynamic impedance Z_h is determined by the buoy parameter. According to maximum power transfer theorem the maximum power can be obtained by matching the PTO impedance Z_u with the hydrodynamic impedance Z_h. Two control strategies are adopted to match the impedance: The passive loading control, where Z_u only includes a resistive component and the value of Z_u equals the absolute value of Z_h. and the complex conjugate control where the Z_u can have the both resistive and reactive component. Z_u is equal to the conjugate of hydrodynamic impedance Z_h. A reactive but not the complex conjugate method is applied in this research. The reactive parts of the impedance are cancelled out, but the resistive parts are not equal.

Table 3.1: Equivalent mechanical quantities to electrical quantities

Mechanical Domain		Electrical Domain	
Quantity	Symbol	Quantity	Symbol
Excitation force	F_e	Source voltage	V_e
Buoy velocity	$\dot{z}$	Current	i
Buoy position	z	Charge	q
WEC total hydrodynamic mass	$M + a_\infty$ or m	Inductance	L_h
Hydrodynamic stiffness	S_b	Capacitance^{-1}	C_h^{-1}
Total buoy damping	R	Resistance	R_h
PTO force	F_u	Load Voltage	V_u
PTO damping	R_u	Load resistance	R_u
PTO spring constant/ PTO added mass	X_u	Load reactance	X_u

The excitation force, spring constant, buoy damping and WEC total mass are the components of hydrodynamic impedance Z_h which are not feasible to control. Hence the PTO impedance Z_u of electric machine is possible to control. The power electronics switching techniques and a control strategy are applied to tune the PTO impedance Z_u so that the Z_u can easily be matched with hydrodynamic impedance Z_h. By applying this method, it is possible to maximize the energy conversion efficiency of the system.

3.2 Operating Principles of the Rack and Pinion based WEC

The PTO force can be calculated according to the electrical analogue that is described in the previous section and it can be represented as

$$F_h = F_e - F_u \tag{21}$$

The left side of (3) represents the hydrodynamic force.

The PTO force develops a torque on the pinions and rotates the pinion in clockwise for each time the rack moves down and counterclockwise when the rack moves up and vice versa. The shaft of the generator rotates in one direction because of the ratcheting method. This method is similar to the rotation method of the bicycle wheel. So, the generator will always experience a unidirectional rotation through the engagement and disengagement of the two one-way bearings that are attached to the two pinions. When the generator shaft speed is equal to or smaller than the pinion speed the system becomes engaged and when the generator shaft speed is greater than the pinion speed then the system becomes disengaged. As a result, the generator is decoupled with the rack and pinion system and rotates due to moment of inertia. The PTO force because of this engagement and disengagement condition can be determined by (1).

The buoy displacement can be calculated using (20). The buoy velocity and the buoy acceleration can be determined by taking the 1st order derivative and 2nd order derivative of the buoy displacement, respectively. A limiter is used to limit the buoy displacement from -0.3m to +0.3m from the reference level of the surface water so that the buoy displacement cannot go beyond the surface of water.

3.3 Control Mechanism of The Rack and Pinion WEC

A reactive control algorithm is adopted to rotate the generator in resonance with the wave excitation force. It keeps the generator rotating at a frequency proportional to the product of wave velocity and the gear ratio. The reference angular velocity is generated by measuring wave excitation force and scaling down with a specific amount. Therefore, the prediction burden of excitation force is eliminated. This reference angular velocity is compared to the generator shaft speed and through a four Quadrant DC chopper, a reference voltage for the machine drive system is set up by the control algorithm [19]. As a result, the generator can rotate continuously in resonance with the wave excitation force. In this way, it is possible to get comparatively higher efficiency of the generator. The control algorithm is mainly consisting of a PI controller for the shaft speed and a PI controller for the armature current. Both of these controllers were tuned using a K-Factor design approach [20]. The block diagram of the control system is shown in Figure 3.2.

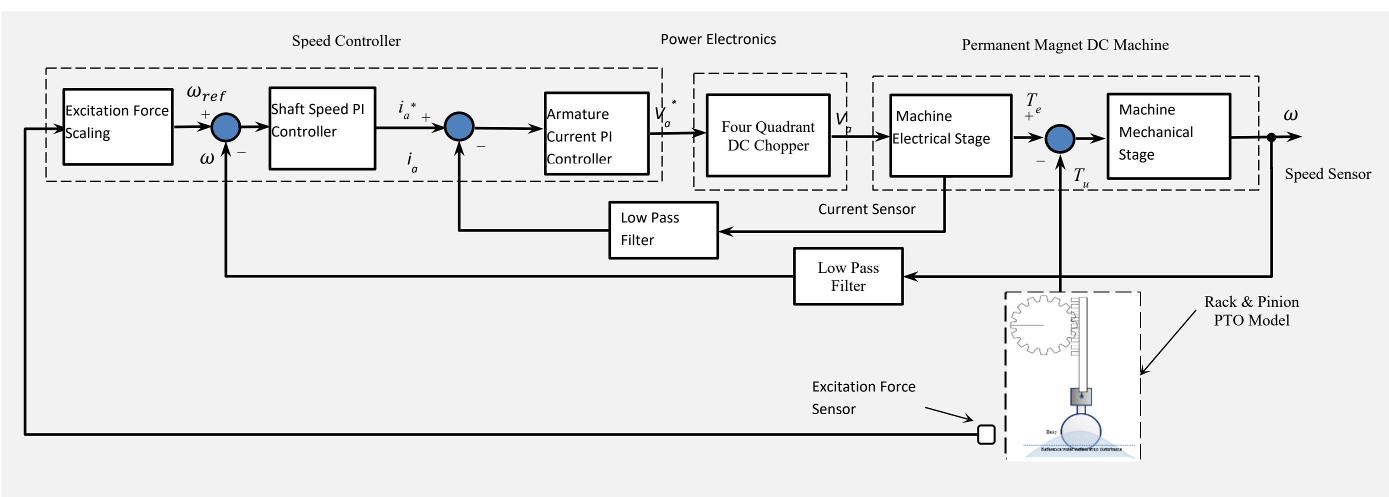

Fig. 3.2. Block diagram of the control system.

3.4 Unidirectional Rotation of Pinion and Generator Shaft

MMR design for wave energy converter application is illustrated in the research paper [5]. Two pinions added with two one-way bearings are mounted on the generator shaft. The working principle of the one-way bearing is analogous to the bicycle gear. The pinions are placed in between two racks. When the rack moves up one pinion gear get engaged with the generator shaft due to the behavior of the one-way bearing, keeping the other pinion inactive. The opposite case happens when the rack moves down. As a result of this mechanism, the generator shaft always experiences one-direction rotational motion.

3.5 Synchronism between wave excitation force and generator shaft speed

The efficiency and the health of a generator depend mostly on the smooth and continuous rotation of the generator shaft [21]. So, it is essential for the rack and pinion WEC system to keep the generator in continuous rotation. The pinion may travel higher angular displacement when the rack moves up compared to the angular displacement when the rack moves down. The pinion may stop rotating at some point, it may also rotate with a different angular velocity that will cause variable generator speed. These situations are not desirable for getting maximum efficiency from the generator.

3.6 Irregular wave processing methodology

Generally, irregular wave consists of numerous regular sinusoidal waves with different wave amplitudes, angular velocities, and phases. The angular frequency is selected from 0 to 2 rad/s with an interval of 0.01 rad/s. The interval is expressed as Δf.

The Pierson-Moskowitz spectrum [22] is used to generate the amplitudes of irregular waves which is a special case of the Joint North Sea Wave Project (JONSWAP) spectrum represented by (22)

$$S(f) = \frac{\alpha_j g^2}{(2\pi)^4} f^{-5} \exp\left[-\frac{5}{4}\left(\frac{f_p}{f}\right)^4\right] \gamma^{\Gamma} \tag{22}$$

where, f_p is the peak frequency of the irregular wave, f is the frequencies of the wave components, γ^{Γ} is the peak enhancement factors. In this research, the value of γ is considered 1 to turn the JONSWAP spectrum into the Pierson-Moskowitz spectrum.

In Equation (22) α_j is a variable of $S(f)$ and if H_{m0} is the significant wave height of the irregular wave then the value of α_j can be determined by Equation (23)

$$\alpha_j = \frac{H_{m0}^2}{16 \int_0^{\infty} S^*(f) df} \tag{23}$$

In the denominator of equation (23), the integrand can be determined as

$$S^*(f) = \frac{g^2}{(2\pi)^4} f^{-5} \exp\left[-\frac{5}{4}\left(\frac{f_p}{f}\right)^4\right] \gamma^{\Gamma} \tag{24}$$

The real time irregular wave data are provided in terms of joint probability distribution and percentage occurrence of each sea state [23]. In the proposed simulation model, The Wave Energy Prize [24] approach is adopted in this thesis for the simplicity of the simulations and six sea states are utilized for the validation of the model in real time environment. The six-sea states along with the weighting function are illustrated in Table 3.2. The data of the six sea states are taken from the wave environment of Newport, Oregon. The integration of Equation (24) is calculated with the limit from 0 to infinity and then the value of α_j is determined for each sea states. The simulations are performed with moment of inertia values of 1.5, 1, 0.5 and 0.1 kg.m^2, gear ratio values of 2.5, 2 and 1.5, and scaling factors ranging from 0.1/5000 to 1/5000 of the excitation wave with a step of 0.05/5000.

The Pierson-Moskowitz spectrum which is equivalent to JONSWAP spectrum [25] with $\gamma = 1$ for the sea state IWS 6 is shown is fig. 3.3.

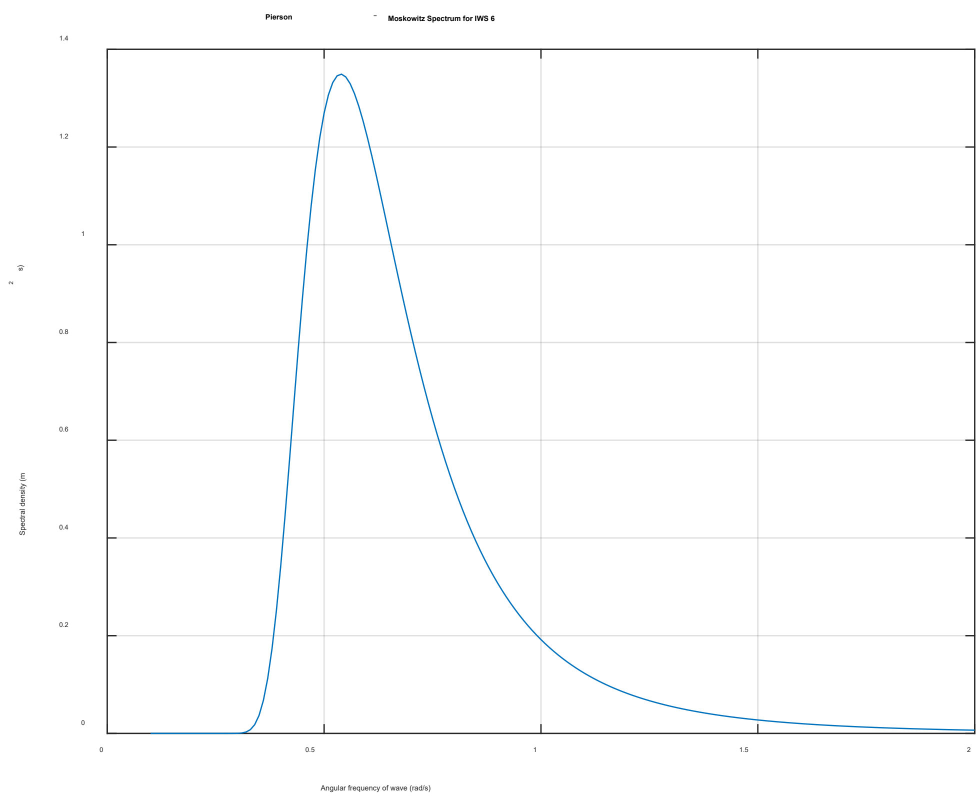

Figure 3.3: An example of sea state with Pierson Moskowitz spectrum.

Table 3.2: Six sea states that are selected for real wave environment

Wave	Tp (s)	Hs (m)	Weighting
IWS 1	7.31	2.34	0.175
IWS 2	9.86	2.64	0.268
IWS 3	11.77	5.36	0.058
IWS 4	12.36	2.97	0.295
IWS 5	15.23	5.84	0.034
IWS 6	16.50	3.25	0.054

The weighting of the sea state represents the probability of occurrence. IWS 4 has the highest percentage of occurrence of 29.5% and the IWS 5 has the lowest percentage of occurrence among the six-sea state which is 3.4%.

CHAPTER 4: RESULTS AND DISCUSSION

4.1 Theoretical Calculation of Maximum Energy Extraction

For the passive loading control, PTO system impedance $Z_u=R_u+jX_u$ becomes purely resistive and its value is given by equation (22),

$$R_u = \sqrt{R^2 + (\omega m - \frac{S_b}{\omega})^2} \tag{22}$$

$$X_u = 0 \tag{23}$$

The passive power transfer is represented by

$$P_{passive} = \frac{F_e^2 R_u}{(R + R_u)^2 + (\omega m - \frac{S_b}{\omega})^2} \tag{24}$$

For the complex conjugate control, the resistive and reactive part of Z_u are

$$R_u = R \tag{25}$$

$$X_u = -\left(\omega m - \frac{S_b}{\omega}\right) \tag{26}$$

According to the maximum power transfer theorem, the maximum power transfer can be calculated by

$$P_{maximum} = \frac{F_e^2}{4R} \tag{27}$$

The maximum mechanical power can be determined by using (24) and (27) for passive loading and complex conjugate control, respectively.

In this research, a complex conjugate or reactive control [26] methodology is applied by keeping buoy velocity and excitation force in phase, which satisfies equation (26). Moreover, buoy velocity amplitude was modified to meet the condition in equation (25).

The maximum rms power transfer for both passive and complex conjugate control can be determined for buoy radius 0.575 m, generator moment of inertia 1 $kg \cdot m^2$, and using regular sinusoidal wave with a constant frequency. If the amplitude of the wave is 0.5 m and the wave period is 5 s then the wave elevation can be represented by

$$z_w = 0.5 \sin\left(\frac{2\pi}{5} t\right) \tag{28}$$

The rms power calculations are shown in Table 4.1, using the rms value of F_e in (24) and (27).

Table 4.1: Theoretical Energy extraction in rms value

Buoy Radius (m)	$P_{passive}$ (kW) for each wave period			$P_{maximum}$ (kW) for each wave period		
	5 s	8 s	10 s	5 s	8 s	10 s
0.575	0.72	0.49	0.39	27.1	88.4	137.8

It is important to note that, the results in Table 4.1 are for a linear PTO system. However, the proposed rack and pinion system is nonlinear due to the engagement and disengagement phenomena. Accordingly, the expectation in this study is to keep the extracted power within these two power boundaries. In addition, there will be some power reduction during the conversion from mechanical power to electrical power due to the losses associated with DC machine operation.

4.2 WEC Model with a DC machine under regular wave conditions

4.2.1 Simulation Model

MATLAB/Simulink^{TM} software is utilized to model the system. The wave excitation force is preprocessed by a MATLAB script and the values are imported into the Simulink model through *toworkspace* platform. The generated electrical power is consumed by a resistance (passive load) or sent to the grid through a four-quadrant DC chopper (active load) respectively. The control algorithm was implemented in the Simulink environment [27].

The pinion speed is always compared with the generator shaft speed. If the pinion speed is greater than or equal to the shaft speed, then the PTO force (F_u) is nonzero. At this moment, the generator is coupled to the buoy. If the pinion speed is less than the shaft speed, then the PTO force (F_u) is zero. In this case, the driving torque for the DC machine is zero. The control algorithm keeps the buoy velocity in resonance with the excitation force and the generator will have a unidirectional speed with a constant average. The power extracted will be investigated at different gear ratios, scaling factor of excitation force, and moment of inertia of the generator. A limiter is used to restrict the displacement of the buoy within the range of −0.3m to +0.3m from the water surface level to ensure a reasonably constant wetness area of the buoy surface [28]. This is important for the applicability of linear potential flow theory.

The simulation is completed in several following steps. First of all, a simulation example is shown with a sample set of tunable parameters. The results of energy extraction and the waveforms of the system during steady-state operation are provided so that the system's feasibility and sufficient energy extraction can be verified. Second, the energy is extracted with different scaling factors of the excitation force and wave periods to verify the system's ability to run stably at various wave periods and scaling factors. Third, the energy extraction is also investigated with various gear ratios and generator moment of inertia to find out what values of these parameters should be selected to extract power stably. The simulation parameters are shown in Table 4.2 and Table 4.3, respectively.

Table 4.2: Mechanical/ Hydrodynamic parameters used in simulation

Parameter	Value
r	0.5m
ρ	1020kg/m2
g	9.81N/kg
R_v	10kg/s
R_f	0

where R_v is the viscous force coefficient and R_f is the friction force coefficient used for hydrodynamic damping.

Table 4.3: Permanent magnet DC machine parameters used in simulations

Parameter	Value
Nominal Speed	1750 rpm
Nominal Power	8.206 kW
Nominal Voltage	480 V
Viscous Friction Coefficient	0 N/(m/s)
Armature Resistance	0.6 Ω
Armature Inductance	0.012 H
Torque Constant	1.8 N.m/A

4.2.2 A Simulation Example

An example of the four-quadrant DC chopper is illustrated in figure 4.1 to verify the system's feasibility and to validate the control algorithm. In this example the wave amplitude is 0.5m, the wave period is 5s, the buoy radius is 0.575m, the gear ratio is 2, the scaling factor is 0.30/5000, and the generator's moment of inertia is 1 $kg \cdot m^2$. In the resonance condition, the average mechanical power and electrical power obtained are 998.2W and 781.2W, respectively. So, the efficiency of the DC machine is 78.26% which indicates that the machine can produce a significant amount of electrical energy. The mechanical power extracted at the same wave period and amplitude is slightly higher than the maximum that is obtained in [5] by tuning the PTO mass and damping parameters.

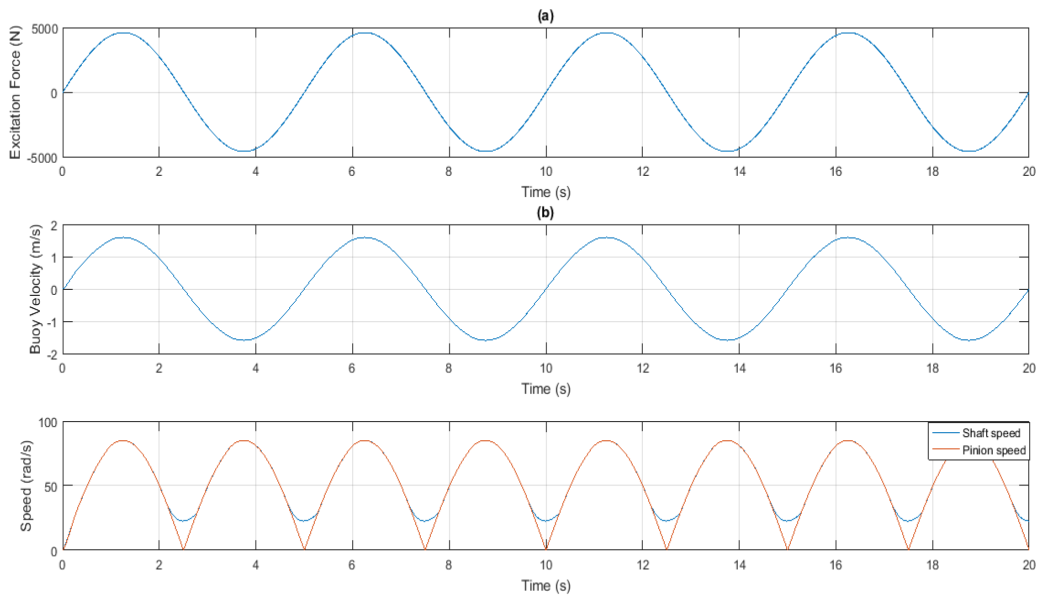

Figure 4.1: (a). Wave Excitation force (b) buoy velocity (c) generator shaft speed (blue) and pinion speed (red).

From figure 4.1 the stability of the system can be perceived, the wave excitation force and the buoy velocity are in resonance with each other, and this can be seen from figure 4.1 (a) and figure 4.1 (b). Generator shaft speed and pinion speed profiles are also quite similar, which is shown in figure 4.1(c). The blue line in figure 4.1 (c) represents the generator shaft speed and the red line represents the pinion speed. The shaft speed and pinion speed are not identical because of the inertia of the generator shaft and exploitation of active load in the external circuit of the generator [29]. When the generator disengages, the speed waveforms are different, and the shaft speed is smoother than the pinion speed.

4.2.3 The Effect of Scaling Factor and Gear Ratio

The simulation results for average electrical power production are summarized in Table 4.4 with the same control methodology. With the increase in gear ratio, the average electrical power decreases. The lowest gear ratio that can be selected for this simulation is 2 because the average power production becomes inconsistent with the system below the gear ratio of 2. However, if the scaling factor is increased, the average electrical power keeps increasing up to a certain value. After that particular value, the generated electrical power keeps decreasing for each wave period. The results are obtained with buoy radius 0.575m, generator moment of inertia 1 $kg \cdot m^2$, and wave periods of 5, 8, and 10 seconds to provide a comparison to the work reported at [5]. The simulation model is able to extract electrical power at these wave periods with the variable scaling factors and gear ratios.

The generation of electrical power varies with the changing of wave periods as shown in Table IV. This simulation generates slightly less maximum power for the time period of 5 seconds as compared to [5] but the maximum power generation for both wave periods 8 seconds and 10 seconds are significantly higher. The combined power for all the three wave periods starts decreasing below the scaling factor 0.35/5000 but only for gear ratio 2 this decrease happens below the scaling factor 0.45/5000. The best selected gear ratio and scaling factor are 3 and 0.35/5000, respectively, for maximum power production of all three combined wave periods.

Table 4.4: Average electrical power at different scaling factor and gear ratio for wave period 5s, 8s and 10s.

Gear ratio	Scaling factor	Electrical power production (W) for each wave period		
		5 sec	8 sec	10 sec
2	0.30/5000	753.5	723.7	696.5

	0.35/5000	781.2	808.2	795.8
	0.40/5000	745.7	860.3	871.8
3	0.30/5000	731.2	701.8	671.1
	0.35/5000	702.5	733.7	720.8
	0.40/5000	635.3	745.7	756.3
4	0.30/5000	673.3	632.1	595.3
	0.35/5000	642.9	649.7	628.4
	0.40/5000	577.9	650.6	649.6
5	0.30/5000	612	582.7	544
	0.35/5000	586	590.7	566.4
	0.40/5000	521.7	583.5	577.9
6	0.30/5000	461	544.8	506.5
	0.35/5000	514.9	546.4	521.4
	0.40/5000	468.8	533.3	526.3

4.2.4 The Effect of Gear Ratio and Generator Moment of Inertia

Table 4.5 illustrates the average electrical power production with different gear ratios and inertia. The simulation was performed at wave periods of 5 seconds, 8 seconds, and 10 seconds, respectively, a buoy radius of 0.575 meter, and a particular scaling factor that provides optimum electrical power. It is clear from Table 4.5 that the maximum electrical power can be related to each inertia.

For a lower gear ratio at a particular buoy size, the system becomes unstable, and the power production will be inconsistent [30]. In this simulation, the optimum power was obtained at gear ratio 2 with each inertia for a wave period of 5 seconds. For wave period 8 sec and 10 sec, the peak power can be achieved at gear ratio 1.5 with inertia 1 $kg \cdot m^2$.

Table 4.5: Maximum average electrical power at different gear ratio and inertia

Inertia ($kg \cdot m^2$)	Gear ratio	Electrical power production (W) for each wave period		
		5 sec	8 sec	10 sec
0.5	1.5	660.3	778.7	921.6
	2	660.8	720.9	771.2
	2.5	631.8	661.8	688.6
1	1.5	772	1070	1817
	2	781.2	890.4	1172
	2.5	759.1	809.5	907
1.5	1.5	660.3	778.7	921.6
	2	660.8	560.4	775
	2.5	631.8	582.2	688.6

The inertia also has an influence on the stability of the system. Very small inertia, as well as large inertia, produces power with unwanted oscillations which can be harmful to the generator. In this case, the optimum power is generated at the inertia of 1 $kg \cdot m^2$.

4.2.5 The Effect of Passive load (Resistor)

The simulation was also carried out using different values of resistance as a passive load to the external circuit of the generator. The same values of buoy radius and wave period are utilized in this case. Table 4.6 shows the results of obtaining average electrical power at various resistance.

Table 4.6: Average electrical energy extraction using passive load

Resistance (Ω)	Average electrical power (W) for each wave period		
	5 sec	8 sec	10 sec
05	568	163.3	109.2
06	102	34.52	17.81
07	75.68	24.99	14.66

The results show that the higher the value of the resistance the lower the average power. The average electrical power reached optimum at resistance 5Ω. The resistance value lower than 5Ω can also produce higher power but the overall system become unstable, and it starts producing power with oscillation. During the passive load testing, it was observed that the phase difference between excitation force and buoy velocity got smaller with decreasing resistance values.

4.3 WEC Model with a DC machine under irregular wave conditions

The wave excitation force for irregular wave is determined by utilizing the method described in Section 2.2.2 and imported those data into the MATLAB/Simulink model. Section 2.2 illustrates the calculation for the hydrodynamic model. A four quadrant DC chopper which works as an active load is used to transfer the WEC power generated to the power supply.

Table 4.7: Mean electrical power extraction at different gear ratio and scaling factor for an irregular wave.

Reference speed scaling factor, k	Mean Electrical Power (W) for Gear Ratio 2.5	Mean Electrical Power (W) for Gear Ratio 2	Mean Electrical Power (W) for Gear Ratio 1.5
0.1/5000	289.9	218.3	167.7
0.15/5000	741.3	749.3	700.6
0.2/5000	1042	1117	1153
0.25/5000	1228	1347	1431
0.30/5000	1322	1470	1571
0.35/5000	1340	1503	1598
0.40/5000	1292	1461	1534
0.45/5000	1186	1351	1423
0.50/5000	1025	1181	1296
0.55/5000	811.6	965	1158

A simulation was performed with the buoy radius 0.575 m, moment of inertia 1 $kg \cdot m^2$, significant wave height of 2 m and the peak period of 5 s. The mean value of electrical power extraction at different scaling factors and three different gear ratios are shown in Table 4.7 to find the maximum electrical power. As the scaling factor keeps increasing the extraction of energy is also increases. At scaling factor 0.30/5000 the power extraction becomes maximum for each gear ratio which are 1340 W, 1503 W, 1598 W for gear ratio 2.5, 2, and 1.5 respectively. After that point power extraction keeps decreasing with the increasing scaling factor.

Below 0.55/5000 scaling factor the power extraction becomes less. The simulation was also performed at peak periods of 8 s, 10 s and 15 s with the similar simulation set up as stated above but the energy extraction was either less or unstable. This problem was related to the machine's limited power rating. In the next set of test cases, a larger machine was used to accommodate these extreme transients in the irregular wave profiles.

The simulation model was also run under real time wave environment to validate the model. The wave environment that is comprised of six sea states from Newport, Oregon (see Table 3.2) was considered to conduct the simulation.

The DC machine was scaled up by doubling the nominal speed and nominal voltage to accommodate the six sea states. The voltage and speed of the DC machine was limited to catch up with the velocity profile which is scaled down version of excitation force. There was no limit for the armature current considering ideal magnetic path for the armature magnet. Energy was extracted under these conditions at three different inertia values of 1.5, 1 and 0.5 kg.m^2, gear ratio values of 2.5, 2 and 1.5, and scaling factors ranging from 0.1/5000 to 1/5000 of the excitation wave with a step of 0.05/5000 for each sea state.

The weighted power results are included in the appendix section in Table B.1, B.2 and B.3. The negative sign in the tables represents power extraction. The weighted extraction of power is consisting of 17.5% of IWS 1, 26.8% IWS 2, 5.8% IWS 3, 2.95% IWS 4, 3.4% IWS 5 and 5.4% IWS 6.

The power extraction increases with the decreasing inertia but there is a realistic limit of inertia of a machine. The lowest inertia is considered 0.5 kg.m^2. At inertia 1.5 kg.m^2 the highest power extraction is obtained at 0.30/5000 scaling factor and 1.5 gear ratio. Figure 4.2 illustrates the 3D plot for weighted power extraction for inertia 1.5 kg.m^2. The maximum power for inertia 1 kg.m^2 is 520.557 W which is obtained at 0.45/5000 scaling factor and 1.5 gear ratio. Inertia 0.5 kg.m^2 provides the highest extraction of electrical power that is 1254.81 W which is obtained at

1/5000 scaling factor and 1.5 gear ratio. Figure 4.3 illustrates the 3D plot for weighted power extraction for inertia 0.5 kg.m^2.

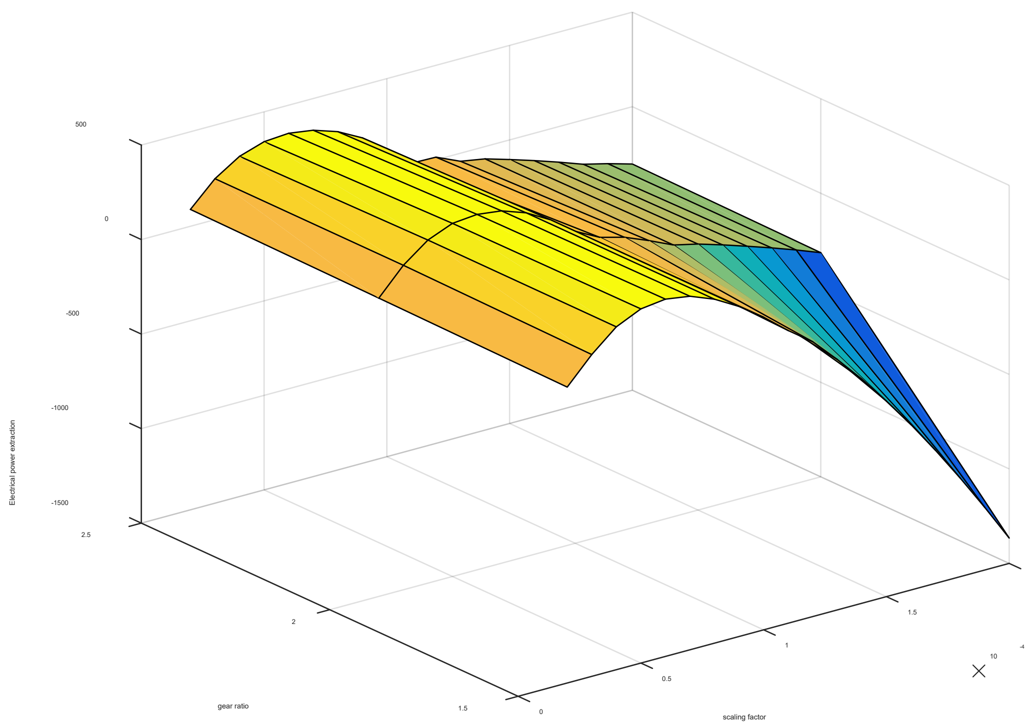

Figure 4.2: Weighted Electrical power extraction for inertia, J=1.5 kg.m^2.

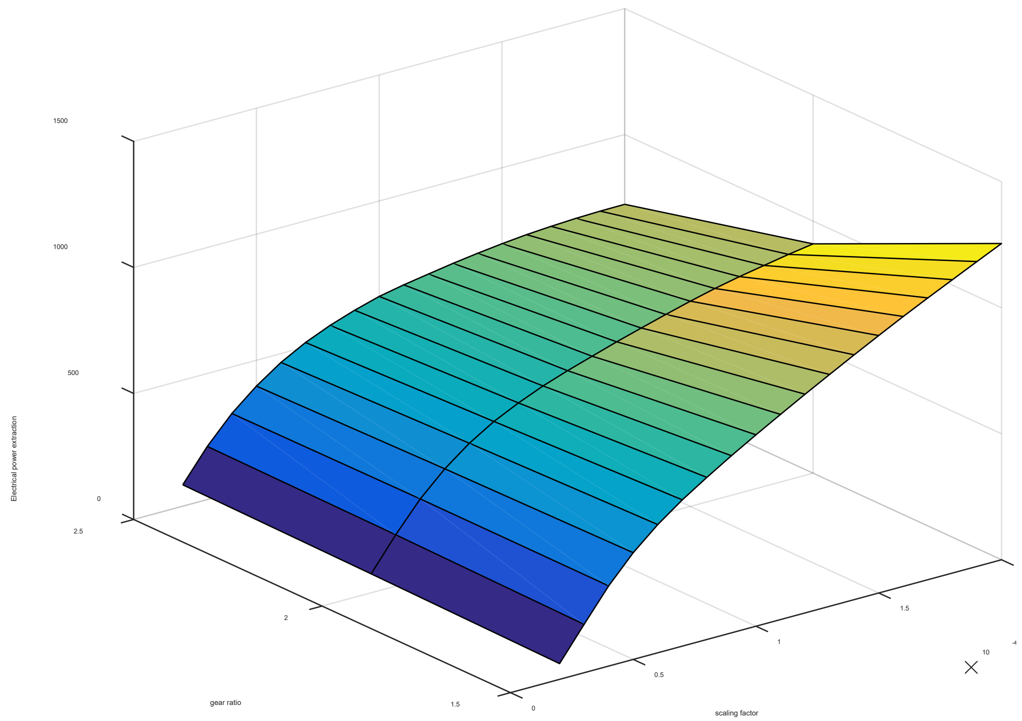

Figure 4.3: Weighted Electrical power extraction for inertia, J=0.5 kg.m^2.

The DC machine's efficiency is also very important to analyze for each sea state [31]. The losses of the DC machine increase with the lower efficiency. Every DC machine has its own loss tolerance capability. Any losses beyond the tolerance level can cause a DC machine ceased to operate.

In case of every gear ratio the efficiency keeps increasing with the increasing scaling factor and peaked at a certain point then it starts decreasing. The highest efficiency for IWS4 is obtained for inertia 0.5 kg.m^2 at gear ratio 2.5 and 0.45/5000 scaling factor. The percentage value of that efficiency is 83.2 %. Figure 4.4 and Figure 4.5 show the variation of efficiency with different gear ratios and scaling factors for inertia J=0.5 kg.m^2 and inertia J=1.5 kg.m^2 respectively. The overall best efficiency value of 85.8% was achieved with IWS6 for inertia 0.5 kg.m^2 at gear ratio 2.5 and 0.45/5000 scaling factor.

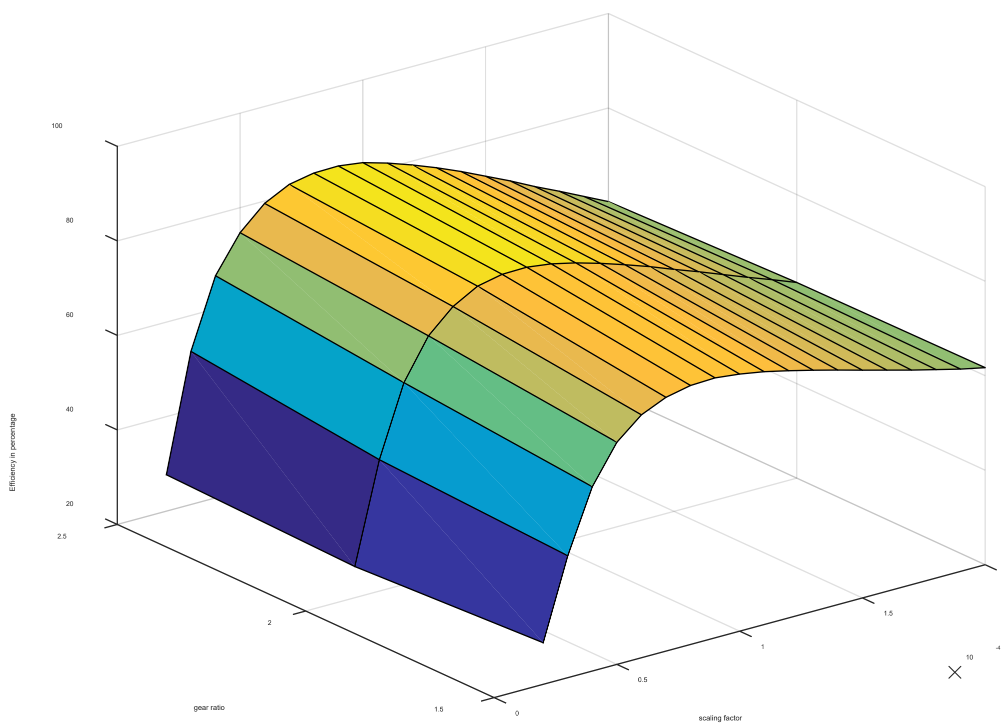

Figure 4.4: Percentage efficiency of power for IWS 4 at inertia, J=0.5 kg.m^2.

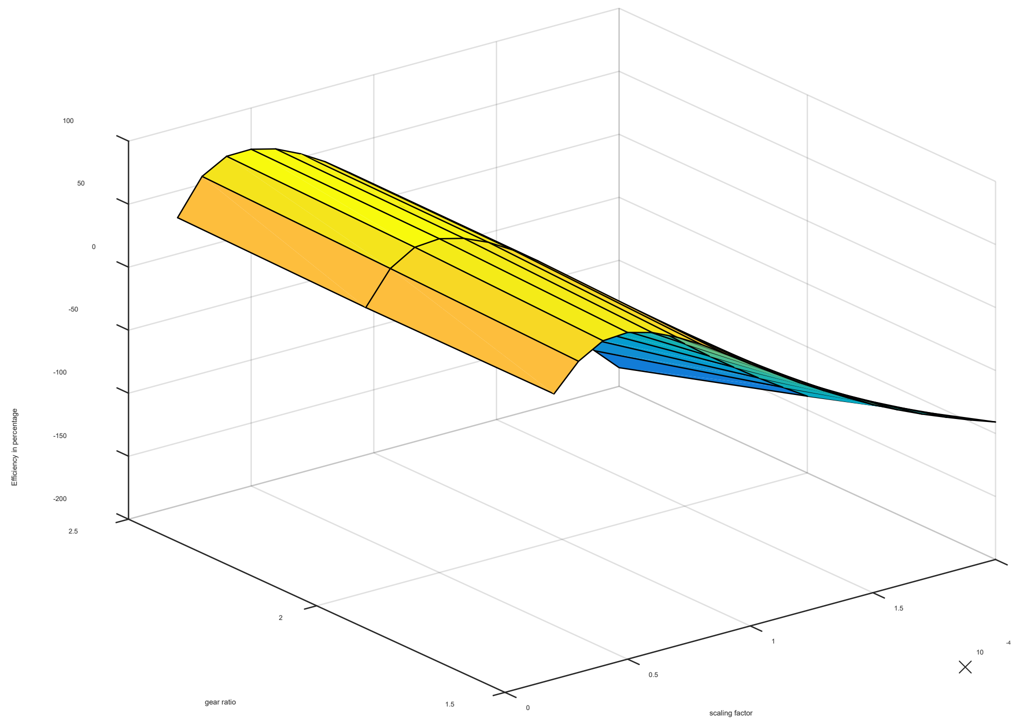

Figure 4.5: Percentage efficiency of power for IWS 4 at inertia, J=1.5 kg.m^2.

The results in the 3D plot can validate that the simulation model can work in real wave environment and it is possible to generate reasonable amount of energy from that model.

The armature current analysis is essential to note in this research. Every DC machine has its own tolerance for its armature current. The armature current tolerance depends on the armature construction and its material. Any current higher than the armature current can damage the conductors of the armature coil. Table 4.8 and Table 4.9 show the armature current of two conditions where the maximum power extraction and the higher efficiency are tracked.

Table 4.8: Peak current for inertia 0.5 kg.m^2 at gear ratio 1.5 and 1/5000 scaling factor

Sea states	Peak current (per unit)
IWS 1	15.98
IWS 2	18.75
IWS 3	42.98
IWS 4	17.91
IWS 5	35.22
IWS 6	14.87

In Table 4.8, the maximum electrical power was obtained at IWS 5. The highest armature current was 42.98 which was obtained at IWS 3.

Table 4.9: Peak current for inertia 0.5 kg.m^2 at gear ratio 2.5 and 0.45/5000 scaling factor

Sea states	Peak current (A)
IWS 1	5.12
IWS 2	6.74
IWS 3	14.84
IWS 4	6.60
IWS 5	12.79
IWS 6	5.76

In Table 4.9, the highest efficiency was achieved at IWS 6 (as mentioned above) and the highest armature current was obtained at IWS 3 which is 14.84. So, the generator can require armature current up to 43 times the nominal value for maximum power extraction. This current is not practical for a real machine and the current needs to be limited. However, the limit is only 5.76 (or 6) times the nominal current considering the highest efficiency point for IWS 6. This clearly shows that the highest efficiency point is more feasible to work with for a practical system implementation.

CHAPTER 5: CONCLUSION AND FUTURE WORK

This thesis presents a control methodology for a rack and pinion based WEC with MMR and power take off system. The excitation force and the buoy velocity are kept in resonance so that the maximum energy can be extracted. The bidirectional rotation of the pinion is converted into unidirectional rotation by MMR to enhance the efficiency of the generator. The control mechanism is novel and does not require predictions of wave excitation force. Simulation results show that a suboptimum average electrical power can be achieved with the selected gear ratio, inertia, and scaling factor of the excitation force. Scaling down the excitation force helps to visualize the system's reaction at different speed of the machine. Limited speed can assist to track the maximum power extraction and optimum efficiency. The system model is also capable of running at different ranges of wave periods and it can generate maximum power stably.

In case of irregular waves, the machine's rating had to be reevaluated to accommodate the extremes in the wave forces. The lower the inertia the higher the electrical power can be obtained but there is a realistic limit of inertia that can be used in the simulation model. Any inertia lower than 0.5 $kg.m^2$ is practically not feasible for a DC machine of given power rating.

This study was aimed at finding trends to obtain larger power and higher efficiency. The parameters evaluated were gear ratio, inertia, and scaling factor of the excitation force. The trend of electrical power extraction and efficiency is similar for $J=1.5\ kg.m^2$ and $J=1.0\ kg.m^2$. For these cases, the peak power and efficiency reaches to a certain point and it starts decreasing from that point with the increase in scaling factor. For $J=0.5\ kg.m^2$, the maximum power extraction was obtained at 1/5000 scaling factor, but the highest efficiency was achieved at scaling factor 0.45/5000 for each gear ratio.

The power extraction increases with the decrease in gear ratio for any inertia. So, the highest power extraction was achieved at 1.5 gear ratio.

In this research, a control strategy was applied to keep the buoy velocity and generator shaft speed in resonance with each other compared to [5]. No control methodology was applied in [5]. The efficiency obtained from the sea state IWS 4 and IWS 6 is higher compared to the overall efficiency both for initial system control strategy and optimized system control strategy described in [32].

The research can be extended to further analysis of other parameters that affect energy extraction. The system performance with irregular wave's parameter such as different significant wave height, buoy radius, peak periods and armature current limiting of DC machine can also be investigated as future work.

REFERENCES

[1] MS. Amin, H. Karayaka, P. Yanik, Y. Sang, "Suboptimal control of a rack and pinion-based wave energy converter power take-off system," *IEEE SoutheastCon Conference 2021*, March 10-14, 2021.

[2] T. Brekken, "Fundamentals of ocean wave energy conversion, modeling and control," in *Proc. IEEE International Symposium on Industrial Electronics (ISIE)*, Bari, Italy, July 4-7, 2010, pp. 3921.

[3] A. Muetze and J. G. Vining, "Ocean Wave Energy Conversion - A Survey," in Proc. Industry Applications Conference - 41st IAS Annual Meeting, vol. 3, pp. 1410-7, 2006.

[4] D.G. Dorrell, J.R. Halliday, P. Miller, and M. Findlater, "Review of wave energy resource and oscillating water column modelling," in Proc. 39th International Universities Power Engineering Conference, vol. 1, pp. 649-53, 2004.

[5] C. Liang, J. Ai, L. Zuo, "Design, fabrication, simulation and testing of an ocean wave energy converter with mechanical motion rectifier," Ocean Engineering, vol. 136, 2017, pp. 190–200.

[6] H. Yavuz, "On control of a pitching and surging wave energy converter," *International Journal of Green Energy*, vol. 8, no. 5, pp. 555{584}, 2011.

[7] K. Rhinefrank, A. Schacher, J. Prudell, T. K. A. Brekken, C. Stillinger, J. Z. Yen, S. G. Ernst, A. von Jouanne, E. Amon, R. Paasch, A. Brown, and A. Yokochi "Comparison of Direct-Drive Power Takeoff Systems for Ocean Wave Energy Applications," IEEE Journal of Oceanic Engineering, vol. 37, no. 1, pp. 35-44, January 2012.

[8] Johannes Falnes, "Ocean Waves and Oscillating Systems," Cambridge University Press 2002.

[9] W.E. Cummins, "The impulse response function and ship motions," Tech Rep., Schiffstechnik, 1962.

[10] A. Hulme, "The wave forces acting on a floating hemisphere undergoing forced periodic oscillations," Journal of Fluid Mechanics, vol. 121, pp. 443–463, 8 1982.

[11] J. Falnes, Ocean waves and oscillating systems: linear interactions oscillations," Journal of Fluid including wave-energy extraction, Cambridge university press, 2002

[12] *Y. Sang et al, "Resonance Control Strategy for A Slider Crank WEC Power Take-off System," in Proc. MTS/IEEE OCEANS '14, St. John's Canada, 2014, pp. 1-8.*

[13] E. Tedeschi, M. Carraro, M. Molinas, and P. Mattavelli, "Effect of control strategies and power take-off efficiency on the power capture from sea waves," *Energy Conversion, IEEE Transactions on*, vol. 26, no. 4, pp. 1088{1098, Dec 2011}.

[14] Hakan Yavuz, “On control of a pitching and surging wave energy converter," *International Journal of Green Energy”*, vol. 8, no. 5, pp. 555{584, 2011}.

[15] A. Kyllingstad, “Approximate analysis concerning wave-power absorption by hydrodynamically interacting buoys," 1982.

[16] T. Bjarte-Larsson, J. Falnes, “Laboratory experiment on heaving body with hydraulic power take-off and latching control”, Ocean Engineering, 33 (2006), pp. 847-877.

[17] Titah-Benbouzid H, Benbouzid M. Ocean wave energy extraction: Up-to-date technologies review and evaluation, in 2014 International Power Electronics and Application Conference and Exposition; 2014. p. 338–42.

[18] E. Tedeschi and M. Molinas, “Tunable control strategy for wave energy converters with limited power takeoff rating," *Industrial Electronics, IEEE Transactions on*, vol. 59, no. 10, pp. 3838{3846, Oct 2012}.

[19] R. Genest, J.V. Ringwood, **“**A critical comparison of model-predictive and pseudospectral control for wave energy devices”, Journal of Ocean Engineering and Marine Energy, 2 (4) (2016), pp. 485-499.

[20] H. D. Venable, “The K-Factor: A new mathematical tool for stability analysis and synthesis,” in Proc. Powercon 10, http://www.venable.biz.

[21] P.B. GarciaRosa, J.P.V.S. Cunha, F. Lizarralde, S.F. Estefen, I.R. Machado, E.H. Watanabe, *“*Wave-to-wire model and energy storage analysis of an ocean wave energy hyperbaric converter”*,* IEEE J Ocean Eng, 39 (2) (2014), pp. 386-397.

[22] OpenEi, WEC Sim: https://openei.org/wiki/File:WEC_Sim_User_Manual_v1.0.pdf. Accessed 06/29/2021.

[23] Y. Yu, N. Tom, and D. Jenne, “Numerical analysis on hydraulic power take off for wave energy converter and power smoothing methods” Proceedings of the 37th International Conference on Ocean, Offshore and Arctic Engineering OMAE 2018 June 17–22, 2018, Madrid, Spain.

[24] Bull, D., and Dallman, A. R., 2017. “Wave Energy Prize Experimental Sea States Selection,” In 36th International Conference on Ocean, Offshore and Arctic Engineering, Trondheim, Norway.

[25] K. Hasselman et al, “Measurements of wind-wave growth and swell decay during the joint North Sea wave project (jonswap),” Tech. Rep., Deutches Hydrographisches Institut, 1973.

[26] J.Hals, T. Bjarte-Larsson, and J. Falnes, “Optimum reactive control and control by latching of a wave-absorbing semi submerged heaving sphere," in *Proc. 21st Int. Conf Offshore Mech. Artic Eng.*, Oslo, Norway, Jun. 2328 2002, pp. 1-9.

[27] J. Hals, J. Falnes, and T. Moan, “Constrained optimal control of a heaving buoy wave energy converter,” Journal of Offshore Mechanics and Arctic Engineering, vol. 133, no.1, pp. 011401,2011.

[28] Kovaltchouk T, Multon B, Ahmed HB, Aubry J, Rongère F, Glumineau A., “Influence of control strategy on the global efficiency of a Direct Wave Energy Converter with electric Power Take-Off”, in 2013 8th International Conference and Exhibition on Ecological Vehicles and Renewable Energies (EVER); 2013. p. 1–10.

[29] Y. Yuan, M. Liu, W.-C. Tai, L. Zuo, “Design and Treadmill Test of a Broadband Energy Harvesting Backpack With a 420 Mechanical Motion Rectifier”, J. Mech. Design 140 (8) (2018) 085001.

[30] Jonkman, J. M., Dynamics Modeling and Loads Analysis of an Offshore Floating Wind Turbine, Ph.D. Thesis, Department of Aerospace Engineering Sciences, University of Colorado, Boulder, CO, 2007; NREL/TP-500-41958, Golden, CO: National Renewable Energy Laboratory.

[30] K. Hasselman et al, “Measurements of wind-wave growth and swell decay during the joint North Sea wave project (jonswap),” Tech. Rep., Deutches Hydrographisches Institut, 1973.

[31] J.V. Ringwood, G. Bacelli, F. Fusco, “Energy-maximizing control of wave-energy converters: The development of control system technology to optimize their operation” IEEE Control Systems, 34 (5) (2014), pp. 30-55.

[32] T. Andersen, H. Pedersen, “Model based design of efficient power take-off systems for wave energy converters,” The Twelfth Scandinavian International Conference on Fluid Power, May 18-20, 2011, Tampere, Finland.

Appendix

APPENDIX A: SOURCE CODE

A.1 Wave Excitation Force Calculation for Regular Wave

A.1.1 Main Code

```
clear;clc;close all;
%=====================================================================%
% initial inertia: 1
% initial viscous friction coefficient: 0.32

%=====================================================================%
%Callback for the simulink model
Ts=2e-3; % Sampling time
Td=1e-3; % Discrete Sampling time

%%% setting 1 %%%
gr=110;    % Gear ratio
%======================
aa=Ts/(.5+Ts);
bb=Td/(.25+Td);


%=====================================================================%
%==========================Initialization===========================%

% global Interval A B J L_af V_f r_f I_f L_aa r_a kv m R Sb

%Hydrodynamics initialization
Start_Time=0;           % time start
End_Time=200;              % final time
Interval=0.01;          % simpling time interval
rho=1020;               % the density of water
g=9.81;                 % acceleration of gravity
a=1.15/2;               % buoy radius
Rv=10;                  % Viscous force coefficient
Rf=0;                   % Friction force coefficient

A=0.5;                  % The maximum amplitude of ocean wave
f=1/5;                  % The frequency of ocean wave
Tp=1/f;                 % Time period of ocean wave
omega=2*pi*f;           % The angular velocity of ocean wave
k=omega^2/g;            % Wave number for infinite water depth
Kaq=k*a;                % ka

zw=@(t)A*sin(omega*t);    % The function of regular sinusoidal ocean wave
```

```
%Rack and Pinion initialization

B=0.01;                 % Viscous friction.
J=1;                   % inertia of pinion.

mcrp=10;                % Total of mass of rack and pinion respectively.



%Generator initialization
L_af = 1.234; % Mutual inductance between the field and the rotating armature coils.
V_f = 220; % Field voltage.
r_f = 150; % Resistance of field windings
I_f = V_f/r_f; % Current of field windings
L_aa = 0.016; % Self-inductance of the field and armature windings.
r_a = 0.78;  % Resistance of the armature coils.
kv = L_af*I_f; % Stator constant

%==================================================================%
%===Calculating mu, epsilon and kappa through graphical observation======%

Ka=[0 0.05 0.1 0.2 0.3 0.4 0.5 0.6 0.7 0.8 0.9 1.0 1.2 1.4 1.6 1.8 2.0 2.5 3.0 4.0 5.0 6.0 7.0 8.0
9.0 10.0]';
Amass=[0.8310 0.8764 0.8627 0.7938 0.7157 0.6452 0.5861 0.5381 0.4999 0.4698 0.4464
0.4284 0.4047 0.3924 0.3871 0.3864 0.3884 0.3988 0.4111 0.4322 0.4471 0.4574 0.4647 0.4700
0.4740 0.4771]';
Damping=[0 0.1036 0.1816 0.2793 0.3254 0.3410 0.3391 0.3271 0.3098 0.2899 0.2691 0.2484
0.2096 0.1756 0.1469 0.1229 0.1031 0.0674 0.0452 0.0219 0.0116 0.0066 0.0040 0.0026 0.0017
0.0012]';

kappa(1)=1;
for i=2:length(Ka)
   kappa(i)=sqrt(4*Damping(i)/(3*pi*Ka(i)));
end

Mu = interp1(Ka,Amass,Kaq','pchip');
Ep = interp1(Ka,Damping,Kaq','pchip');
kap= interp1(Ka,kappa,Kaq','pchip');

%==================================================================%
%Calculating Coefficients of the Differential Equation of Buoy Displacement

Sb=rho*g*pi*a^2;%785890;
mm=rho*(2*pi/3)*a^3;
m=mm*(1+Mu);%267040+156940;
R=Rv+Rf+Ep*omega*mm;%91520;
```

```
Fe=@(t)kap*rho*g*pi*a^2*zw(t);
t = Start_Time:Interval:End_Time;

figure;
% subplot(2,1,1)
% plot(t,eta);
% grid
% title('wave elevation')

% subplot(2,1,2)
plot(t,Fe(t));
grid
title('excitation force')
% hold on;
figure;
plot(t,zw(t));
grid
title('wave elevation')
Ocean_Wave_AccP.signals.values=Fe(t)';
Ocean_Wave_AccP.time=t';

%Call to find Wave Analysis
Wave_Analysis;
```

A.1.2 Wave Analysis

```
% ============Output==============
% T_s are the half periods
% T1_s are the time point of zero-crossings
Excitation_Force=Ocean_Wave_AccP.signals.values;
Ocean_Wave_AccP.time=Ocean_Wave_AccP.time;
l_Fe=length(Excitation_Force);
i_T=1;
for index=2:l_Fe
   if Excitation_Force(index)*Excitation_Force(index-1)<=0  %0-crossing detection
      if Excitation_Force(index)>Excitation_Force(index-1)
         pn_flag(i_T)=1;
      else pn_flag(i_T)=0;
      end
      T1_s(i_T)=t(index-1);
      if i_T>1
         T_s(i_T)=T1_s(i_T)-T1_s(i_T-1);
      else
         T_s(i_T)=0;
      end
      i_T=i_T+1;
   end
```

end

A.1.3 Simulink Model

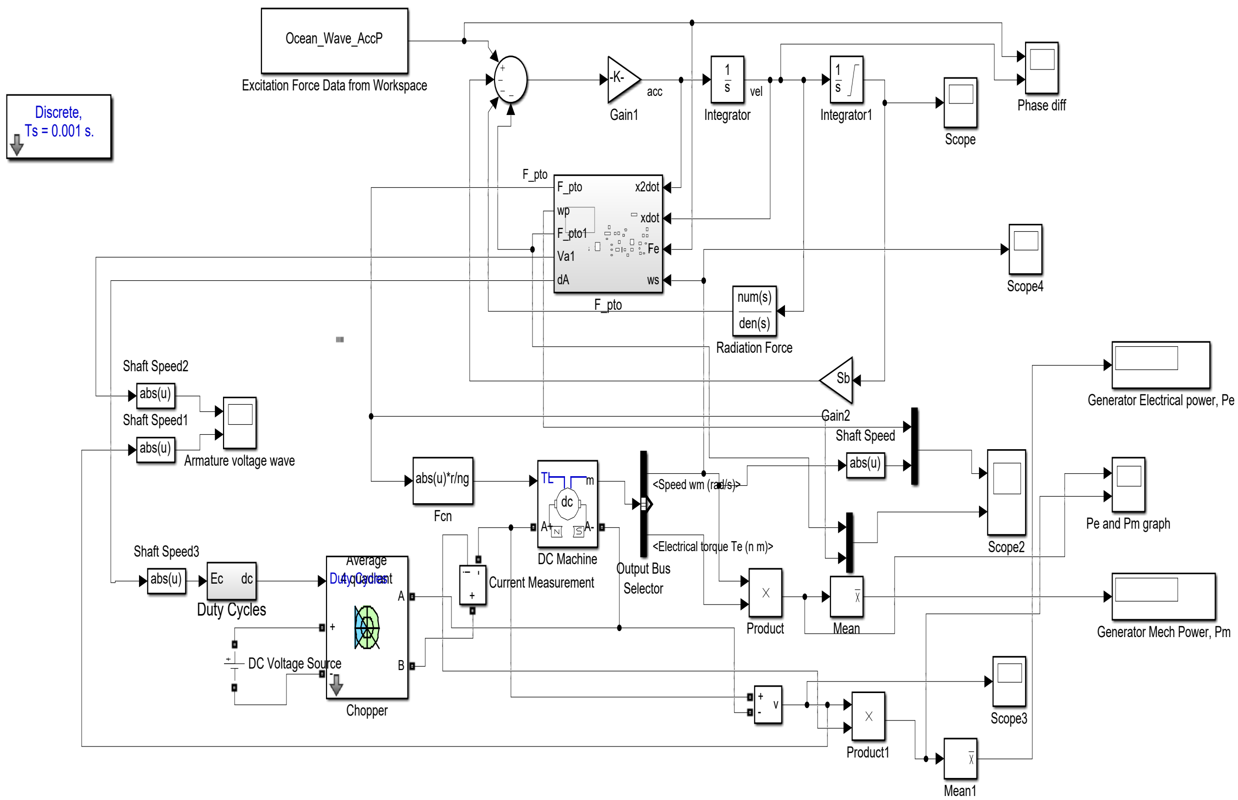

Figure A.1: Simulink model for regular waves.

A.1.4 Details of the F_pto Block

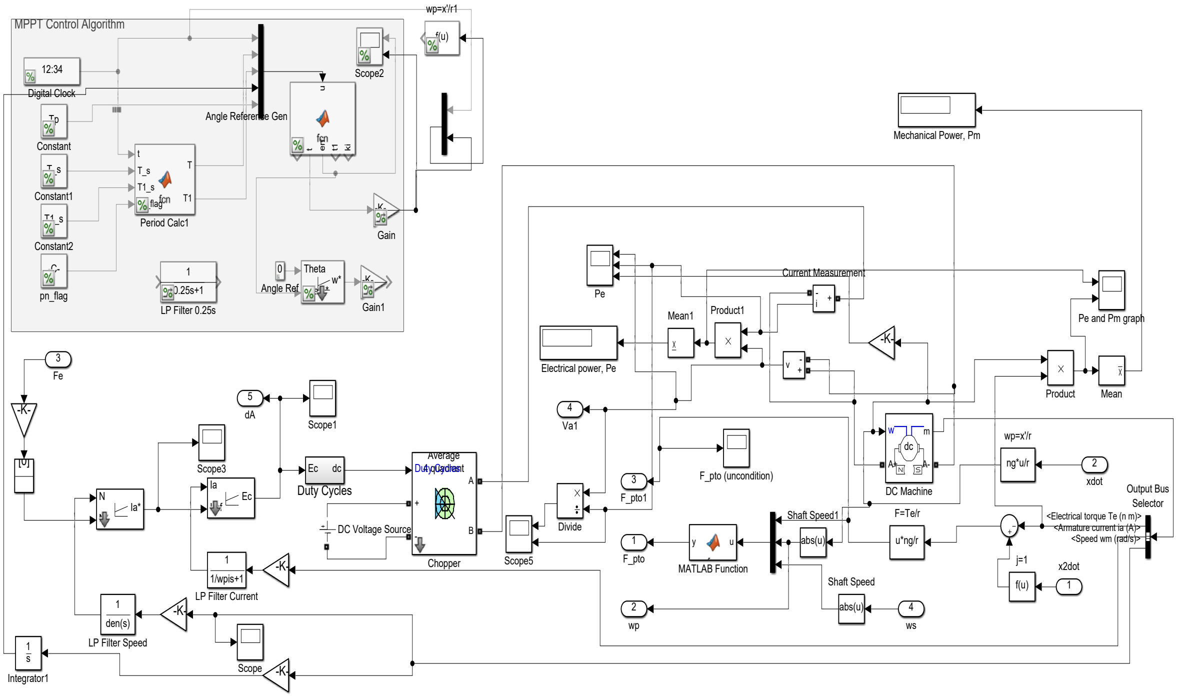

Figure A.2: Details of the F_pto Block for regular waves.

A.1.5 Radiation Force Calculation

File Name: RadiationKomega

```
%clear;clc;close all;
function [bz,az,bs,as]=RadiationKomega(a,Td)
%=====================================================================%
%============================Initialization===========================%


%Hydrodynamics initialization
rho=1020;             % the density of water
g=9.81;               % acceleration of gravity

%a=5;%0.9533;          % buoy radius
%A=0.5;                % The maximum amplitude of ocean wave.

Rv=0;                 % Viscous force coefficient
Rf=10;                % Friction force coefficient
```

```
omega=0:0.01:4.4; %when w > 4.4 then ka > 10 in which we don't have damping data to
interpolate for


l2=length(omega);

m=zeros(l2,1);
R=zeros(l2,1);
K=zeros(l2,1);

Ka=[0 0.05 0.1 0.2 0.3 0.4 0.5 0.6 0.7 0.8 0.9 1.0 1.2 1.4 1.6 1.8 2.0 2.5 3.0 4.0 5.0 6.0 7.0 8.0
9.0 10.0]';
Amass=[0.8310 0.8764 0.8627 0.7938 0.7157 0.6452 0.5861 0.5381 0.4999 0.4698 0.4464
0.4284 0.4047 0.3924 0.3871 0.3864 0.3884 0.3988 0.4111 0.4322 0.4471 0.4574 0.4647 0.4700
0.4740 0.4771]';
Damping=[0 0.1036 0.1816 0.2793 0.3254 0.3410 0.3391 0.3271 0.3098 0.2899 0.2691 0.2484
0.2096 0.1756 0.1469 0.1229 0.1031 0.0674 0.0452 0.0219 0.0116 0.0066 0.0040 0.0026 0.0017
0.0012]';
mm=rho*(2*pi/3)*a^3;
minf=0.5;

for j2=1:l2%2*pi*f;            % The angular velocity of water wave

    k=omega(j2)^2/g;            % Wave number for infinite water depth
    Kaq=k*a;                % ka

    %zw=@(t)A*sin(omega(j2)*t);    % the function of Ocean wave



%================================================================%
    %===Calculating mu, epsilon and kappa through graphical observation======%


    Mu = interp1(Ka,Amass,Kaq','pchip');
    Ep = interp1(Ka,Damping,Kaq','pchip');
    %kap= interp1(Ka,kappa,Kaq','pchip');


%================================================================%
    %Calculating Coefficients of the Differential Equation of Buoy Displacement

    m(j2)= mm*(Mu-0.5);
    R(j2)= Rv+Rf+Ep*omega(j2)*mm;
```

```
    K(j2)= R(j2)+1i*omega(j2)*m(j2);

end

% mag=abs(K);
% phase=angle(K);
[bs,as] = invfreqs(K,omega,3,4);
% [bz,az] = invfreqz(mag.*exp(j*phase),omega,3,4);
%impulse(tf(b,a)); %Compare with your RIRF
sysc=tf(bs,as)
sysd=c2d(sysc,Td);
[bz1,az1]=tfdata(sysd);
bz=cell2mat(bz1);
az=cell2mat(az1);
end
```

A.2 Wave Excitation force calculation for irregular wave

A.2.1 Main Code

```
clear;clc;close all;
%==================================================================%
% initial inertia: 1
% initial viscous friction coefficient: 0.32

%==================================================================%
%Callback for the simulink model
Ts=2e-3; % Sampling time
Td=1e-3; % Discrete Sampling time

%%% setting 1 %%%
gr=110;    % Gear ratio
%=====================
aa=20e-6/(.5+20e-6);

%==================================================================%
%Rack and pinion initialization
r=0.0375  %.5;                  % Radius of Pinion
B=0.01;                 % Viscous friction, used again in the slider crank function.
J=1; %10;                  % inertia of flywheel, used again in the slider crank function.
mcrp=10;                % Total of mass of rack and pinion respectively.

%==================================================================%
% Hydrodynamics initialization (frequency domain)
delta_omega=0.01;
omega=0.1:delta_omega:2;
```

```
N=length(omega);
fn=omega/2/pi;% frequencies of the wave components
%%%=============================================%%%
%%% Settings for irregular wave parameters %%%
% Equivalent energy transfer: Hm0=2*sqrt(2)*A  (A is the amplitude of the regular wave)
Hm0=2; %*sqrt(2); %1;%% significant wave height of the irregular wave. The same value is
used as that in "Effect of..."
Tp=10; % If this changes, int_S_star has to be recalculated. Peak period of the irregular wave. In
"Effect of...", they used an average period of 6. We can use our own to make the spectrum fit our
need.
%%%=============================================%%%
fp=1/Tp;
g=9.81; % gravity acceleration
rho=1020;% water density
a=1.15/2;%0.9533;              % buoy radius
Rv=10;                % Viscous force coefficient
Rf=0;                 % Friction force coefficient

%omega=1;                % The angular velocity of water wave
A=0.5;                 % The maximum amplitude of water wave, initialized again in the slider
crank function.
f=1/5;                 % The frequency of water wave
Tp=1/f;
%==================================================================%
% Choose Spectrum for the System:
flag = 1; % 0 for Breschneider model and 1 for JONSWAP Model

switch flag
   case 0
% =====================  Bretschneider model  ============================%
%        R=(Tp/1.057)^(-4); % These are calculated separately for the sake of the organing the
formula
%        Q=R*Hm0^2/4;% These are calculated separately for the sake of the organing the
formula
%        S=Q*fn.^(-5).*exp(-R*fn.^(-4)); % Bretschneider spectrum ("sea spectra revisited" or
MIT OCW slides)
       S=Hm0^2/4*(1.057*fp)^4*fn.^(-5).*exp(-5/4*(fp./fn).^4); %According to
WEC_Sim_User_Manual_v1.0.pdf
   case 1
% =====================  JONSWAP Model
===================================%
       m0=sqrt(Hm0/4); % wave field variance. See "On control ...".
       %alpha=0.0081; % a given constant which is used in most references, see "sea spectra
revisited".
```

```
gamma=6;% If this changes, int_S_star has to be recalculated. The average of gamma is 3.3 (see "sea spectra revisited"). enhancement factor by which the P_M peak energy is multiplied to get the peak energy value of the spectrum.
    %Increasing gamma has the effect of reducing the spectral bandwidth,
    %thereby increasing periodicity of the wave field. See "On control ...".
    for i2=1:N
        if fn(i2)<=fp
            sigma=0.07;%if f<fp  sigma is the width factor of the enhanced peak, see "sea spectra revisited". The numbers are given in "sea spectra revisited".
        elseif fn(i2)>fp
            sigma=0.09;%if f>fp
        end

%=====================================================================%
        % the following eqn is from On Control of a Pitching and Surging Wave Energy Converter-HYavuz.pdf
        %     S(i2)=5*m0/fp*((fp/fn(i2))^5)*exp(-5/4*((fp/fn(i2))^4))*gamma^exp(-(fn(i2)/fp-1/(2*sigma^2)));

%=====================================================================%
        % the following eqn is from sea_spectra_revisited.pdf and Measurements of wind-wave growth and swell decay during the Joint North Sea Wave Project (JONSWAP)_Jonswap-Hasselmann1973.pdf
        %     S(i2)=alpha*g^2*(2*pi)^(-4)*fn(i2)^(-5)*exp(-5/4*((fp/fn(i2))^4))*gamma^exp(-(fn(i2)-fp)^2/(2*sigma^2*fp^2));

%=====================================================================%
        % The following eqn uses basic spectrum from "On control ..." and peak enhancement factor from "Sea_spectra_revisited".
        S(i2)=5*m0/fp*((fp/fn(i2))^5)*exp(-5/4*((fp/fn(i2))^4))*gamma^exp(-(fn(i2)-fp)^2/(2*sigma^2*fp^2));

%=====================================================================%
        % The following eqn is according to WEC_Sim_User_Manual_v1.0.pdf
        % integral of
        % 9.81^2/(2*pi)^4*x^(-5)*exp(-5/4*(0.125/x)^4)*6^exp(-((x/0.125-1)/(sqrt(2)*0.07))^2)
        % from 0 to 0.125 = 37.61 calculated by Wolframalpha
        % integral of
        % 9.81^2/(2*pi)^4*x^(-5)*exp(-5/4*(0.125/x)^4)*6^exp(-((x/0.125-1)/(sqrt(2)*0.09))^2)
        % from 0.125 to infinity=65.8056 calculated by Wolframalpha
        switch Tp
            case 5
            % Integrate the following two items
            % 9.81^2/(2*pi)^4*x^(-5)*exp(-5/4*((1/5)/x)^4)*6^exp(-((x/(1/5)-1)/(sqrt(2)*0.07))^2)
```

```
            % 9.81^2/(2*pi)^4*x^(-5)*exp(-5/4*((1/5)/x)^4)*6^exp(-((x/(1/5)-
1)/(sqrt(2)*0.09))^2)
            int_S_star=5.73884+ 10.0411;
            case 6
               int_S_star=11.9001+20.8213;
            case 7
               int_S_star=22.0463+38.574;
            case 8
               int_S_star=37.61+65.8056;
            case 9
               int_S_star=60.244+105.408;
            case 10
               int_S_star=91.8214+160.658;
            case 15
               int_S_star=464.846+813.332;
            % Integrate the following two items
            % 9.81^2/(2*pi)^4*x^(-5)*exp(-5/4*((1/15)/x)^4)*6^exp(-((x/(1/15)-
1)/(sqrt(2)*0.07))^2)
            % 9.81^2/(2*pi)^4*x^(-5)*exp(-5/4*((1/15)/x)^4)*6^exp(-((x/(1/15)-
1)/(sqrt(2)*0.09))^2)
         end
         alpha=Hm0^2/(int_S_star*16); %int_S_star should be changed when Tp or gamma
changes.
         GAMMA=exp(-((fn(i2)/fp-1)/(sqrt(2)*sigma))^2);
         S(i2)=alpha*g^2/(2*pi)^4*fn(i2)^(-5)*exp(-5/4*(fp/fn(i2))^4)*gamma^GAMMA;
      end
end
 plot(omega,S)
 xlabel('Angular velocity (radian/s)');
 ylabel('Spectral density (m^2/s)');
 grid on;
%=================================================================%
% Wave elevation and excitation force (time domain)
Start_Time=0;          % time start
End_Time=500;           % final time
Interval=0.01;          % sampling time interval
t=Start_Time:Interval:End_Time;
M=length(t);

%%% setting 2 %%%
%a=1.15/2; %5; % buoy radius
%======================
c=rho*g*pi*a^2; % a coefficient that is used later
%%% setting 3 %%%
A=sqrt(2*S*delta_omega/2/pi); % calculate amplitude for each wave component
```

```
rng(0); %Define the seed for next two calls for random numbers

%======================
%%% setting 5 %%%
Phase=2*pi*rand(1,N); % randomly generate the initial phase of each wave component
%======================
A=A+(Hm0/(2*sqrt(2)*1000))*randn(size(S));

Ka=[0 0.05 0.1 0.2 0.3 0.4 0.5 0.6 0.7 0.8 0.9 1.0 1.2 1.4 1.6 1.8 2.0 2.5 3.0 4.0 5.0 6.0 7.0 8.0
9.0 10.0]';
Amass=[0.8310 0.8764 0.8627 0.7938 0.7157 0.6452 0.5861 0.5381 0.4999 0.4698 0.4464
0.4284 0.4047 0.3924 0.3871 0.3864 0.3884 0.3988 0.4111 0.4322 0.4471 0.4574 0.4647 0.4700
0.4740 0.4771]';
Damping=[0 0.1036 0.1816 0.2793 0.3254 0.3410 0.3391 0.3271 0.3098 0.2899 0.2691 0.2484
0.2096 0.1756 0.1469 0.1229 0.1031 0.0674 0.0452 0.0219 0.0116 0.0066 0.0040 0.0026 0.0017
0.0012]';
len=length(Ka);
kappa=zeros(1,len);
imkap=zeros(1,len);
rekap=zeros(1,len);
mm=rho*(2*pi/3)*a^3;
Sb=rho*g*pi*a^2;%785890;
kappa(1)=1;
imkap(1)= 2*Damping(1)*Ka(1)/3;
rekap(1)= sqrt(kappa(1)^2-imkap(1)^2);
for j=2:len
   kappa(j)= sqrt(4*Damping(j)/(3*pi*Ka(j)));
   imkap(j)= 2*Damping(j)*Ka(j)/3;
   rekap(j)= sqrt(kappa(j)^2-imkap(j)^2);
end

Kaq=omega.^2/g*a;
kappa_im=zeros(1,N);
kappa_re=zeros(1,N);
kappa_angle=zeros(1,N);
kappa_abs=zeros(1,N);
for i1=1:N
   kappa_abs(i1)=interp1(Ka,kappa,Kaq(i1),'cubic');
   kappa_im(i1)=interp1(Ka,imkap,Kaq(i1),'cubic');
   kappa_re(i1)=interp1(Ka,rekap,Kaq(i1),'cubic');
   kappa_angle(i1)=atan(kappa_im(i1)/kappa_re(i1));
end
%%%
% kap=0.502764572022028;
%%%
% eta=zeros(1,M);
```

```
% Fe=zeros(1,M); % initialization for wave force at each time point
Fe=@(t)0;
eta_total=@(t)0;
%%% setting 5 %%%
% omega=2*pi/6*ones(1,N);
% kappa_angle=0;
%======================
for i=1:N
   eta{i}=@(t)A(i)*sin(omega(i)*t+Phase(i)+kappa_angle(i));
   Fe_components{i}=@(t)c*kappa_abs(i)*eta{i}(t);
   Fe=@(t)Fe(t)+Fe_components{i}(t);
   eta_total=@(t)eta_total(t)+eta{i}(t);
end
%
Fe=@(t)kap*rho*g*pi*a^2*(eta{1}(t)+eta{2}(t)+eta{3}(t)+eta{4}(t)+eta{5}(t)+eta{6}(t)+eta{7
}(t)+eta{8}(t)+eta{9}(t)+eta{10}(t));%zw(t);

% for i=1:M
%     eta(i)=sum(A.*sin(omega*t(i)+Phase));
%     Fe(i)=sum(c*kappa_abs.*A.*sin(omega*t(i)+Phase+kappa_angle));
% end
figure;
% subplot(2,1,1)
% plot(t,eta);
% grid
% title('wave elevation')

% subplot(2,1,2)
plot(t,Fe(t));
grid
title('excitation force')
% hold on;
figure;
plot(t,eta_total(t));
grid
title('wave elevation')
Ocean_Wave_AccP.signals.values=Fe(t)';
Ocean_Wave_AccP.time=t';
%save ExFcC1 Ocean_Wave_AccP
Theta_Initial=0; %Initial_Angle_Solver();
[bz,az,bs,as]=RadiationKomega(a,Td);
```

```
%Call to find Wave Analysis
Wave_Analysis;
```

A.2.2 Wave Analysis

```
% =============Output==============
% T_s are the half periods
% T1_s are the time point of zero-crossings
Excitation_Force=Ocean_Wave_AccP.signals.values;
Ocean_Wave_AccP.time=Ocean_Wave_AccP.time;
l_Fe=length(Excitation_Force);
i_T=1;
for index=2:l_Fe
    if Excitation_Force(index)*Excitation_Force(index-1)<=0  %0-crossing detection
        if Excitation_Force(index)>Excitation_Force(index-1)
            pn_flag(i_T)=1;
        else pn_flag(i_T)=0;
        end
        T1_s(i_T)=t(index-1);
        if i_T>1
            T_s(i_T)=T1_s(i_T)-T1_s(i_T-1);
        else
            T_s(i_T)=0;
        end
        i_T=i_T+1;
    end
end
```

A.2.3 Radiation Force Calculation

File Name: RadiationKomega

```
%clear;clc;close all;
function [bz,az,bs,as]=RadiationKomega(a,Td)
%=================================================================%
%==========================Initialization===============================%


%Hydrodynamics initialization
rho=1020;               % the density of water
g=9.81;                 % acceleration of gravity

%a=5;%0.9533;                % buoy radius
%A=0.5;                  % The maximum amplitude of ocean wave.

Rv=0;               % Viscous force coefficient
Rf=10;                  % Friction force coefficient
```

```
omega=0:0.01:4.4; %when w > 4.4 then ka > 10 in which we don't have damping data to
interpolate for


l2=length(omega);

m=zeros(l2,1);
R=zeros(l2,1);
K=zeros(l2,1);

Ka=[0 0.05 0.1 0.2 0.3 0.4 0.5 0.6 0.7 0.8 0.9 1.0 1.2 1.4 1.6 1.8 2.0 2.5 3.0 4.0 5.0 6.0 7.0 8.0
9.0 10.0]';
Amass=[0.8310 0.8764 0.8627 0.7938 0.7157 0.6452 0.5861 0.5381 0.4999 0.4698 0.4464
0.4284 0.4047 0.3924 0.3871 0.3864 0.3884 0.3988 0.4111 0.4322 0.4471 0.4574 0.4647 0.4700
0.4740 0.4771]';
Damping=[0 0.1036 0.1816 0.2793 0.3254 0.3410 0.3391 0.3271 0.3098 0.2899 0.2691 0.2484
0.2096 0.1756 0.1469 0.1229 0.1031 0.0674 0.0452 0.0219 0.0116 0.0066 0.0040 0.0026 0.0017
0.0012]';
mm=rho*(2*pi/3)*a^3;
minf=0.5;

for j2=1:l2%2*pi*f;          % The angular velocity of water wave

    k=omega(j2)^2/g;           % Wave number for infinite water depth
    Kaq=k*a;              % ka

    %zw=@(t)A*sin(omega(j2)*t);   % the function of Ocean wave



%=================================================================%
    %===Calculating mu, epsilon and kappa through graphical observation======%


    Mu = interp1(Ka,Amass,Kaq','pchip');
    Ep = interp1(Ka,Damping,Kaq','pchip');
    %kap= interp1(Ka,kappa,Kaq','pchip');


%=================================================================%
    %Calculating Coefficients of the Differential Equation of Buoy Displacement

    m(j2)= mm*(Mu-0.5);
```

```
        R(j2)= Rv+Rf+Ep*omega(j2)*mm;
        K(j2)= R(j2)+1i*omega(j2)*m(j2);

end

% mag=abs(K);
% phase=angle(K);
[bs,as] = invfreqs(K,omega,3,4);
% [bz,az] = invfreqz(mag.*exp(j*phase),omega,3,4);
%impulse(tf(b,a)); %Compare with your RIRF
sysc=tf(bs,as)
sysd=c2d(sysc,Td);
[bz1,az1]=tfdata(sysd);
bz=cell2mat(bz1);
az=cell2mat(az1);
end
```

A.2.4 Simulink model

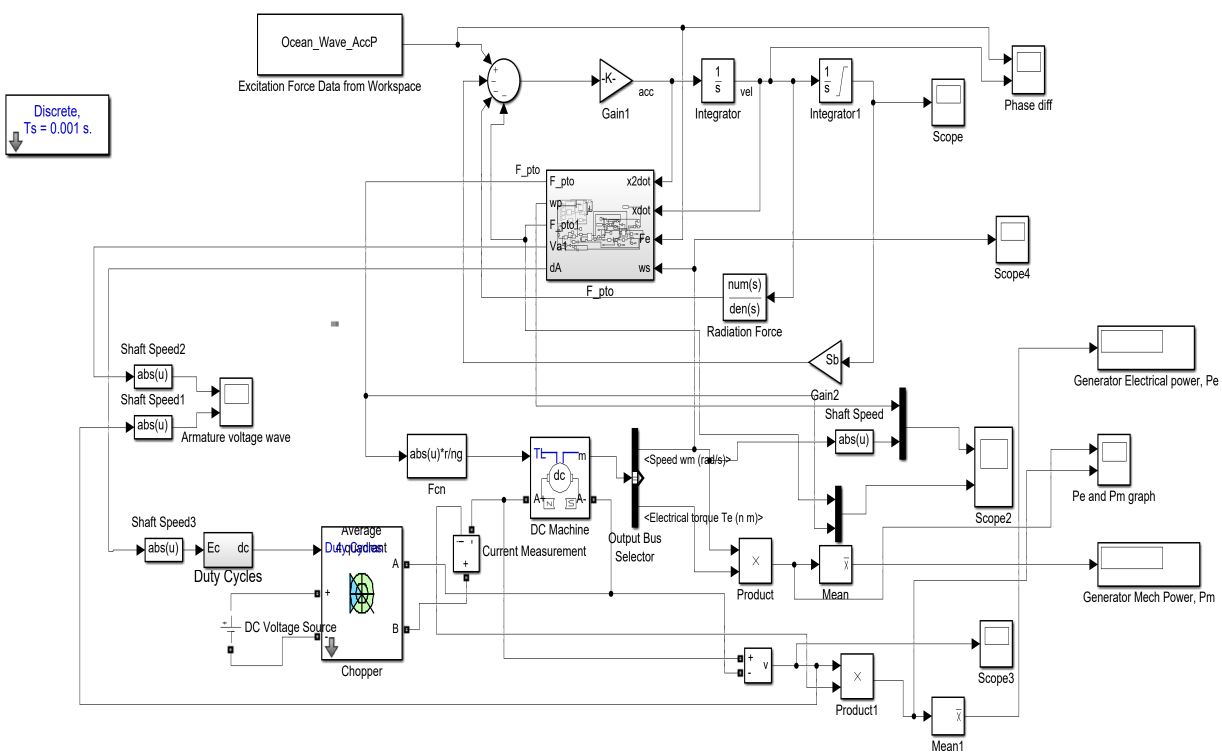

Figure A.3: Simulink Model for irregular waves.

A.2.5 Details of the F_pto Block

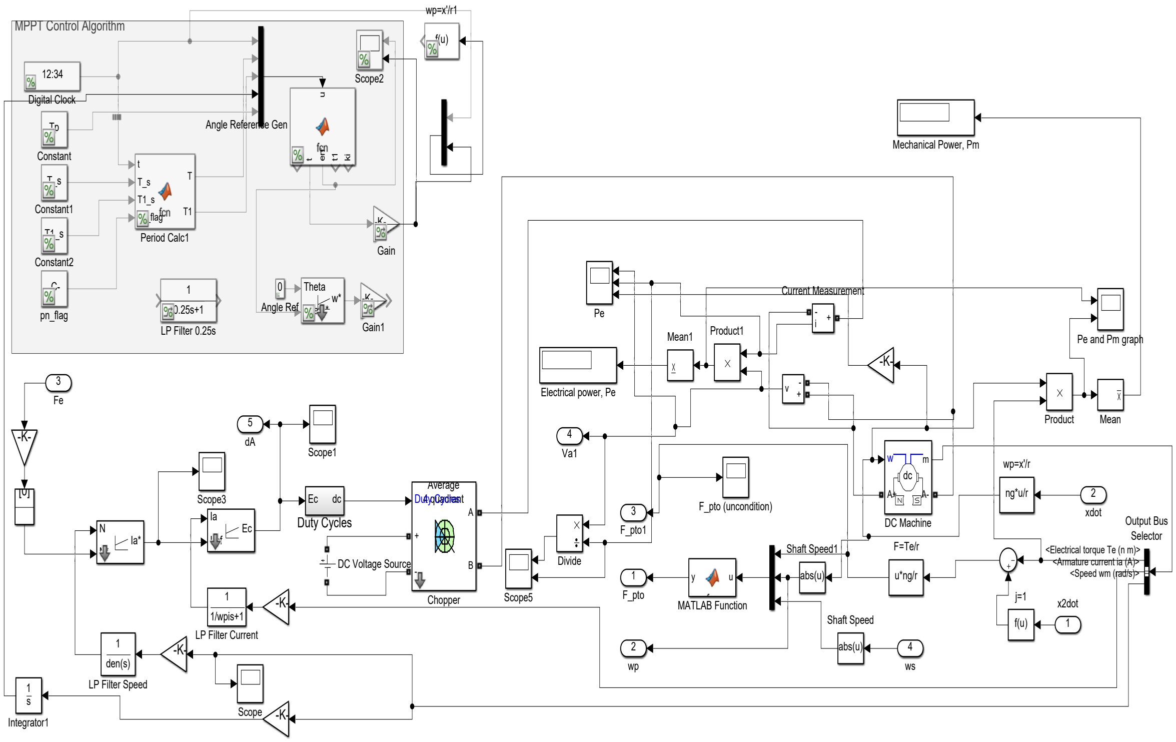

Figure A.4: Details of the F_pto block for irregular waves.

APPENDIX B: WEIGHTED POWER RESULTS WITH IRREGULAR WAVES

Table B.1: Weighted power extraction of six sea states for inertia, J=1.5 Kg.m^2

scaling factor	J=1.5								
	ng=2.5	me, ng=2.5	efficiency	ng=2	me, ng=2	efficiency	ng=1.5	me, ng=1.5	efficiency
0.1/5000	-89.1365	-290.638	30.7	-77.9443	-312.01	25.0	-65.2405	-292.3731	22.3
.15/5000	-216.528	-396.351	54.6	-216.485	-441.912	49.0	-202.347	-483.1338	41.9
0.2/5000	-299.705	-472.122	63.5	-314.8	-527.301	59.7	-313.742	-592.7358	52.9
.25/5000	-341.919	-533.376	64.1	-367.979	-595.442	61.8	-373.524	-673.0082	55.5
.30/5000	-351.395	-585.298	60.0	-380.143	-650.226	58.5	-389.944	-742.2767	52.5
.35/5000	-332.339	-631.058	52.7	-363.795	-702.106	51.8	-370.104	-806.7764	45.9
.40/5000	-289.711	-672.386	43.1	-318.332	-748.12	42.6	-319.333	-868.8889	36.8
.45/5000	-221.836	-709.231	31.3	-246.054	-790.315	31.1	-245.774	-932.7951	26.3
.50/5000	-129.974	-739.874	17.6	-150.236	-829.287	18.1	-153.761	-999.0946	15.4
.55/5000	-17.1972	-768.31	2.2	-82.9723	-870.966	9.5	-48.2108	-1069.9477	4.5
.60/5000	-14.2606	-793.281	1.8	-48.5734	-914.369	5.3	46.2729	-1125.2186	7.9
.65/5000	42.71898	-822.57	-5.2	4.32648	-960.354	-0.5	175.2148	-1199.5431	3.6
.70/5000	65.1755	-853.872	-7.6	62.77208	-1009.89	-6.2	314.6778	-1278.2133	-0.6
.75/5000	103.8195	-886.433	-11.7	92.9315	-1061.96	-8.8	465.6004	-1359.485	-4.7
.80/5000	144.5588	-920.658	-15.7	132.402	-1115.1	-11.9	625.1402	-1443.6635	-8.3
.85/5000	187.941	-955.479	-19.7	174.755	-1169.09	-14.9	796.6236	-1528.2688	-10.4
.90/5000	234.1712	-990.548	-23.6	218.5578	-1223.79	-17.9	977.5752	-1612.3829	-12.5
.95/5000	266.175	-1025.8	-25.9	264.862	-1280.21	-20.7	1167.775	-1702.9258	-14.4
1.0/5000	303.275	-1062.18	-28.6	314.2522	-1337.15	-23.5	1365.931	-1793.6009	-16.3

Table B.2: Weighted power extraction of six sea states for inertia, J=1 Kg.m^2

scaling factor	J=1								
	ng=2.5	me, ng=2.5	efficiency	ng=2	me, ng=2	efficiency	ng=1.5	me, ng=1.5	efficiency
0.1/5000	-88.4511	-288.359	30.7	-77.6026	-302.557	25.6	-64.4135	-279.754	23.0
.15/5000	-219.182	-395.206	55.5	-215.106	-438.76	49.0	-200.769	-471.185	42.6
0.2/5000	-318.567	-472.926	67.4	-327.623	-525.961	62.3	-324.908	-585.727	55.5
.25/5000	-386.78	-535.422	72.2	-406.785	-595.235	68.3	-413.212	-670.746	61.6
.30/5000	-433.21	-590.915	73.3	-459.096	-655.109	70.1	-471.371	-743.186	63.4
.35/5000	-456.289	-635.184	71.8	-486.081	-704.403	69.006	-503.217	-808.875	62.2
.40/5000	-461.173	-674.472	68.4	-494.296	-750.818	65.834	-519.502	-877.329	59.2
.45/5000	-454.2	-713.749	63.6	-489.804	-798.187	61.4	-520.557	-947.263	55.0
.50/5000	-435.306	-751.904	57.9	-472.3	-845.722	55.8	-512.814	-1021.81	50.2
.55/5000	-404.287	-788.675	51.3	-442.686	-892.947	49.6	-496.654	-1099.85	45.2
.60/5000	-361.684	-824.008	43.9	-405.651	-942.917	43.0	-473.276	-1181.96	40.0
.65/5000	-308.431	-857.937	36.0	-361.522	-995.048	36.3	-443.373	-1267.9	35.0
.70/5000	-248.555	-894.209	27.8	-309.732	-1048.63	29.5	-409.811	-1359.2	30.2
.75/5000	-207.599	-931.895	22.3	-251.973	-1104.51	22.8	-369.826	-1453.53	25.4
.80/5000	-159.979	-969.614	16.5	-188.724	-1161.8	16.2	-325.76	-1550.6	21.0
.85/5000	-107.005	-1006.67	10.6	-119.394	-1219.64	9.8	-274.675	-1649.16	16.7
.90/5000	-94.8368	-1043.35	9.1	-45.5265	-1278.85	3.6	-219.972	-1746.85	12.6
.95/5000	-60.0837	-1081.38	5.6	34.2352	-1338.48	-2.6	-160.568	-1851.58	8.7
1.0/5000	-23.2967	-1121.61	2.1	118.3054	-1399.87	-8.5	-97.7438	-1954.67	5.0

Table B.3: Weighted power extraction of six sea states for inertia, J=0.5 $Kg.m^2$

scaling factor	J=0.5								
	ng=2.5	me, ng=2.5	efficiency	ng=2	me, ng=2	efficiency	ng=1.5	me, ng=1.5	efficiency
0.1/5000	-84.7931	-282.703	30.0	-74.99967	-289.204	25.9	-62.49246	-264.784	23.6
.15/5000	-210.869	-392.344	53.7	-203.8182	-428.971	47.5	-191.9185	-366.608	52.3
0.2/5000	-315.0677	-471.255	66.9	-319.7175	-519.888	61.5	-318.2367	-572.465	55.6
.25/5000	-397.4505	-534.835	74.3	-412.682	-591.963	69.7	-423.4033	-663.892	63.8
.30/5000	-464.9292	-589.968	78.8	-487.8826	-653.704	74.6	-508.72	-740.677	68.7
.35/5000	-517.6014	-637.794	81.2	-547.9074	-706.779	77.5	-580.4223	-812.382	71.4
.40/5000	-559.1472	-679.403	82.3	-595.1025	-754.37	78.9	-643.278	-883.935	72.8
.45/5000	-592.8404	-717.523	82.6	-636.0349	-802.506	79.3	-702.8547	-959.864	73.2
.50/5000	-621.3099	-756.524	82.1	-670.2949	-850.441	78.8	-759.3684	-1039.59	73.0
.55/5000	-640.9563	-791.447	81.0	-701.2355	-900.453	77.9	-814.035	-1123.54	72.5
.60/5000	-657.2173	-827	79.5	-732.0504	-955.136	76.6	-867.7666	-1211.86	71.6
.65/5000	-673.1207	-866.041	77.7	-760.3825	-1011.3	75.2	-919.8316	-1303.47	70.6
.70/5000	-686.7287	-906.318	75.8	-787.8737	-1070.05	73.6	-971.3332	-1398.68	69.446
.75/5000	-698.5407	-947.588	73.7	-814.2742	-1131.4	72.0	-1021.4978	-1497	68.236
.80/5000	-708.2613	-989.702	71.6	-838.2505	-1193.39	70.2	-1070.7999	-1597.55	67.0
.85/5000	-714.8827	-1031.15	69.3	-858.985	-1254.64	68.5	-1118.0395	-1699.77	65.8
.90/5000	-719.7781	-1073.22	67.1	-876.901	-1316.07	66.6	-1163.9475	-1804.37	64.5
.95/5000	-722.539	-1115.36	64.8	-894.4253	-1379.39	64.8	-1209.572	-1913.15	63.2
1.0/5000	-723.2118	-1157.77	62.5	-909.8112	-1443.02	63.0	-1254.805	-2021.11	62.1